LITHOS 446-447 (2023) 107132

Contents lists available at ScienceDirect

LITHOS

journal homepage: www.elsevier.com/locate/lithos

Causes, effects, and implications of the relationships amongst fluids, serpentinisation, and alloys

K.A. Evans [a,c,*], B.R. Frost [b], S.M. Reddy [a,c], T.C. Brown [b]

[a] School of Earth and Planetary Sciences, Curtin University, GPO Box U1987, Perth, WA 6845, Australia
[b] Department of Geology and Geophysics, University of Wyoming, Laramie, WY, USA
[c] John de Laeter Centre, Curtin University, GPO Box U1987, Perth, WA 6845, Australia

ARTICLE INFO

Keywords:
Ultramafic
Serpentinisation
Alloy
Awaruite
PGE
PGM

ABSTRACT

Diverse assemblages of metal alloys occur within ultramafic rocks from a wide range of tectonic settings and geological environments. Alloys are typically small and can be difficult to find and identify, but they can host Re and Os, which are significant for geochronology, as well as other elements of economic interest, and can act as catalysts that help to form organic compounds.

The alloys typically form from elements that show chalcophile and siderophile characteristics, indicating that alloys generally form under reducing, S-poor conditions. These conditions can be generated by a range of mechanisms that differ amongst alloy-forming environments, but include desulfidation during melting, exsolution from magmatic S-bearing phases during melt crystallisation, auto-hydrothermal, and sub-solidus processes involving a reduction in fS_2, and electron transfer processes related to serpentinisation.

Alloy formation during serpentinisation is typically associated with the formation of a companion phase that hosts Fe^{3+}, such as Fe^{3+}-bearing serpentine, magnetite, ferrit-chromite, or andradite, recording disproportionation of Fe^{2+} released by olivine alteration to form Fe^0 and Fe^{3+}. An additional source of electrons for alloy formation is provided by the reduction of H^+ in water to H_2, and the reduction of water activity couples with a reduction in fS_2, driving desulfidation reactions and facilitating alloy formation. Other electron donors, such as methane, may also contribute to alloy formation. Alloy-forming serpentinites are strongly internally-buffered, but can follow a range of trajectories through compositional space.

Serpentinite-hosted alloys offer opportunities to better understand a range of geological processes with applications within earth and material sciences. However, these advances require new thermodynamic data and activity composition models for all but the most common alloys, and better characterisation of alloy compositions.

1. Introduction

Ultramafic rocks commonly contain metal alloys (e.g., Beard and Hopkinson, 2000; Frost, 1985; Lorand and Luguet, 2016; O'Driscoll and Gonzalez-Jimenez, 2016). The most common alloys are Fe-Ni alloys, including awaruite (Ni_3Fe), wairauite (CoFe), native Cu, Au-bearing alloys, and a range of PGE-bearing alloys. The PGE alloys host Re and Os, which are used for geochronology (e.g., Becker and Dale, 2016; Harvey et al., 2016) and document early Earth and its evolution (e.g., Day et al., 2016). Most alloys form only at low oxygen (fO_2) and sulfur (fS_2) fugacities, so they provide a sensitive record of the intensive parameters that dominate during early serpentinisation (e.g., Beard and Hopkinson, 2000; Foustoukos et al., 2015; Frost, 1985). Awaruite may act as a catalyst for serpentinisation reactions (Neto-Lima et al., 2015), contributing to abiogenic synthesis of organic compounds, including methane (e.g., Horita and Berndt, 1999; McCollom and Seewald, 2001; Sleep et al., 2004), with implications for the formation of early life. The H_2 that is commonly associated with awaruite formation is also, potentially, an excellent catalyst for the formation of organic compounds (McCollom and Seewald, 2006).

Alloys provide resources of elements of economic interest (Ni, PGEs) (e.g., Beinlich et al., 2020; Britten, 2017). The PGEs have long been mined from alloys and other platinum-group minerals (PGMs), but awaruite is gaining attention as a Ni-resource (e.g., Britten, 2017; Seiler

* Corresponding author at: School of Earth and Planetary Sciences, Curtin University, GPO Box U1987, Perth, WA 6845, Australia.
E-mail address: k.evans@curtin.edu.au (K.A. Evans).

https://doi.org/10.1016/j.lithos.2023.107132
Received 24 October 2022; Received in revised form 2 March 2023; Accepted 10 March 2023
Available online 16 March 2023

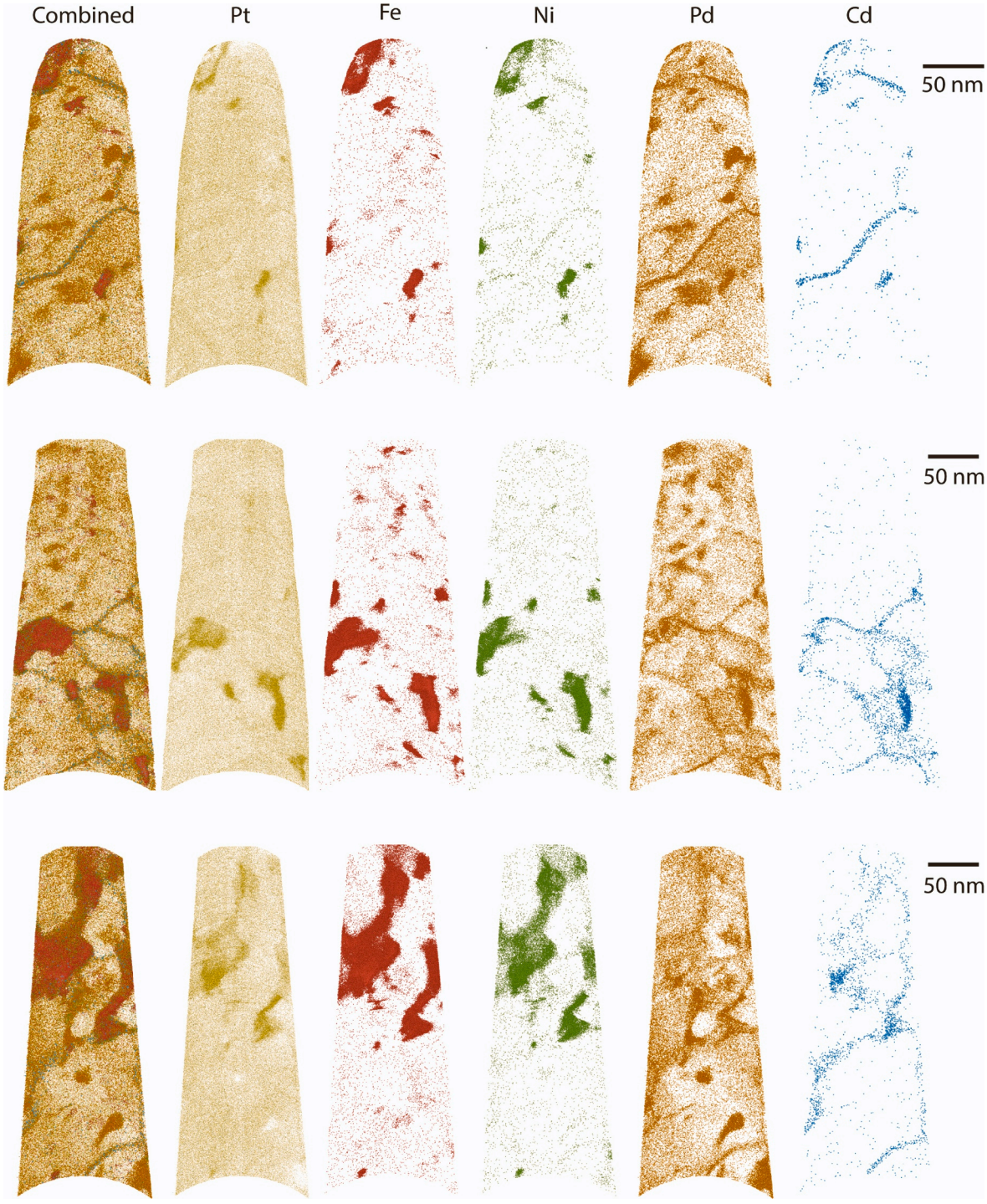

Fig. 1. Atom probe reconstructions of three Cu-Pt alloy specimens from Macquarie Island showing elemental distributions of Pt, Fe, Ni, Pd and Cd and the combined elemental data. The dominant element in all specimens (Cu) is not shown. For clarity, some trace elements are omitted and the reconstructions show a 10 nm slice through the full atom probe reconstruction. For Fe, Ni and Pd, 50% of atoms are shown, 20% of Pt atoms are shown and 100% of Cd atoms are shown. Details of the sample and analytical methods are provided by Evans et al. (in press).

et al., 2022). Alloys may also play a role in environmental rehabilitation after mining and geosequestration of atmospheric CO_2; tailings from awaruite mining provide capacity for CO_2-sequestration and are sulfide-poor, limiting their potential to produce acid mine drainage (e.g., Britten, 2017; Harrison et al., 2013). The catalytic potential of awaruite for C-bearing reactions is likely to prove beneficial in these applications.

Apart from josephinite, which may occur in nuggets as large as 40 kg (Dick, 1974; Jamieson, 1905), most alloy grains are micron-scale or smaller, so they can be difficult to find and identify, but their value as a source of geological information and economically, and the increasing spatial resolution and ever-decreasing detection limits of modern geochemical techniques have motivated detailed studies of the composition and distribution of alloys within rocks from a wide range of geological settings (e.g., Britten, 2017; Evans et al., 2017; Frost et al., 2013; Gonzalez-Jimenez et al., 2010; Klein et al., 2009; Nozaka, 2003; O'Driscoll and Gonzalez-Jimenez, 2016). The increasing spatial resolution available for analysis of alloy grains has revealed significant nanometre-scale heterogeneity (e.g., Daly et al., 2017; Evans et al. in

Table 1
Compilation of awaruite occurrences. See also Eckstrand (1975).

Location	AW	PN	HZ	MT	CU	PGA	Significant other phases	EQ	Citation
Experimental									
Experiment	x		x	x				2	Filippidis, 1985
Experiment	x			x				2	Filippidis, 1985
Abyssal Serpentinites									
Samail Ophiolite	x			x			Fe-rich brucite Fe-rich serpentine	2	Ellison et al., 2021
Mid-Atlantic Ridge	x	E		L?				3	Klein and Bach, 2009
Santa Elena Ophiolite, Costa Rica	x	x	T	x	x		Cu-sulfides Pyrrhotite	3	Schwarzenbach et al., 2014
Iberian abyssal plain, Spain	x	E	x				Fe-rich brucite Co-rich pentlandite	3	Beard and Hopkinson, 2000
Iberian abyssal plain, Spain	x	E					Andradite	3	Beard and Hopkinson, 2000
Ultramafic intrusions									
Dumont Sill, Quebec, Canada	x		x	x				3	Eckstrand, 1975
Dumont Sill, Quebec, Canada	x	E, x	E, L	x				3	Sciortino et al., 2015
Chromitites									
Hengenshan Sill, China	x		x		L		Brucite	3	Jiang and Zhu, 2020
East Sayan, Siberia	x	x	x	x		x	Orcelite	1	Kiseleva et al. 2014
Dobromirtsi Ultramafic Massif, Bulgaria	x	E	x				Godlevskite Arsenides	2	Gonzalez-Jimenez et al., 2010
Chromitites, Southern New South Wales, Australia	x	E		L		x	Trevorite(L) Millerite Polydymite	2	Graham et al., 1996
Suture zone ophiolite									
Baptiste Deposit, Cache Creek Formation, British Columbia, Canada	x	x		x				3	Britten, 2017
Baptiste Deposit, Cache Creek Formation, British Columbia, Canada	x	E	E					3	Britten, 2017
Sakhakot-Qila Complex, Pakistan	x	x	x			x	Ir-rich awaruite	1	Ahmed and Bevan, 1981
Malenco peridotite, Italy	x	E	x	x	x			3	Peretti et al., 1992
Ophiolitic rocks, Jamaica	x	E	x	L	L			3	Scott et al. 2009
East Sayan, Siberia	x					x	Carbonaceous material	1	Zhmodik et al., 2004
Supra-subduction zone ophiolite									
Josephine Ophiolite	X	X		X	X		Taenite, andradite, pyrrhotite, chalcopyrite, chalcocite sphalerite, Ni-arsenides	3	Ramdohr, 1950, Dick, 1974, Botto and Morrison, 1976.
New Caledonia	x	x	x	x		x		3	Evans et al., 2017
Ouen Island, New Caledonia	x	E	x	x		x	Native Ni	2	Gonzalez-Jiminez et al. 2011
Dun Mountain, New Zealand	x	x	E	x	x		Wairauite	3	Brathwaite et al., 2017
La Cabana, Chile	x	E	x	L				3	Gonzalez-Jimenez et al., 2021
Canyon Mountain Ophiolite, Oregon, USA	x			T			Ferric-rich serpentine	3	Evans et al., 2009
Subducted serpentinite									
La Cabana, Chile	x	E	x					3	Gonzalez-Jimenez et al., 2021
Contact Metamorphosed									
Chonguku District, Japan, Zone 1	x			x				3	Nozaka, 2003
Chonguku District, Japan, Zone 2	E	x		x				3	Nozaka, 2003
Chonguku District, Japan, Zone 3	E	x	x	x				3	Nozaka, 2003

Abbreviations: AW = awaruite; PN = pentlandite; HZ = heazlewoodite; MT = magnetite; CU = native Cu; PGA = PGE alloys; E = pre-awaruite; L = post-awaruite; T = Trace; EQ = Reliability of assemblage reporting (1: Insufficient detail; 2: Mostly complete; 3: Reliable with photomicrographs showing key textural relationships and lists of stable assemblages.

press; Parman et al., 2015), which helps to resolve significant questions around the multiple processes that form and modify alloys with ultramafic rocks.

Geological alloy-forming processes are diverse and include, but are not limited to, pre-differentiation processes on early Earth, high temperature processes within Earth's mantle, and low temperature processes related to serpentinisation and weathering. The PGEs and other alloy-forming elements such as Fe, Ni, and Cu can act as either chalcophile or siderophile elements, a property that requires intermediate electronegativity and a capacity to form covalent or metallic bonds. Alloys form in environments where the sulfur fugacity (fS_2) is insufficient to form sulfides (e.g., Schwarzenbach et al., 2014). This can be achieved by melting or desulfidation of base-metal sulfides (BMS), the latter of which can occur at high or low temperatures (e.g., Fonseca et al., 2012). The fS_2 relates to S solubility in silicate melts or aqueous fluids, which are a complex function of pressure, temperature, fluid composition, and oxygen fugacity (fO_2), so the relative stabilities of alloys and sulfides also depend on these parameters in a complex way.

A number of reviews have focussed on the formation of PGE-bearing alloys during magmatic processes (e.g., Lorand and Luguet, 2016; O'Driscoll and Gonzalez-Jimenez, 2016), so this contribution focuses on PGE- and Fe-Ni, Co alloys that form within ultramafic rocks during hydration, the conditions that are required to form them, and the geological processes that provide those conditions. Current challenges within this research field and opportunities for further work are highlighted.

2. Issues with sampling and recognition

Alloys can be small, often less than ten microns, and sometimes on the nanometre-scale, and are commonly rare, particularly the PGE-bearing alloys, because PGE concentrations within ultramafic rocks are relatively low, typically of the order of a few ppb (Salters and Stracke, 2004). For this reason, PGMs and other small alloys can be found more easily if several thin sections are cut, using calculations of the expected size and frequency of grains for typical or known PGE

concentrations to determine a sensible number (Crossley et al., 2020). It can also be useful to apply automated mapping techniques based on back-scattered-electron image brightness (e.g., Evans et al., 2017).

The small size of alloys also poses challenges for analysis. Laser ablation–inductively coupled plasma–mass spectroscopy (LA–ICP–MS) is commonly used to analyse minerals because this technique offers low detection limits and rapid quantitative analysis for a wide range of major and trace elements. However, it can be difficult to obtain appropriate standards for PGE-bearing alloys, and the typical spot size is of the order of several tens of microns, which is much larger than most alloy grains. For this reason, LA–ICP–MS analysis is likely to sample a mixture between alloy grains and hosting or adjacent minerals, and this must be deconvoluted to obtain a robust analysis of the alloy grain. Nevertheless, useful results can be obtained by this technique; Foustoukos et al. (2015) identified fine scale exsolution and Pt alloy formation in a pentlandite grain by LA–ICP–MS.

Electron microprobe analysis (EPMA) has the advantage of a smaller spot-size than LA–ICP–MS but the detection limits are higher, of the order of hundreds to thousands of parts per million, which can be prohibitively high if the concentrations of PGEs within base-metal alloys are required. Synchrotron-based X-ray techniques are used to analyse alloy phases (e.g., Daly et al., 2017), and the high energy of the X-ray beam provides the advantages of low detection limits and the capacity to detect and analyse alloy grains below the surface of the prepared sample. However, quantitative analysis by this technique can be problematic, and the spatial resolution, while much better than that of LA–ICP–MS, is on the micron to ten-micron length-scale on most synchrotrons, so features smaller than this cannot be characterized without specialist beamline equipment. Scanning nuclear microprobes can also reveal and characterize alloy grains hidden beneath the sample surface, with sampling depths of up to 70 μm (Alard et al., 2011).

Techniques that use the magnetic properties, rather than the chemical composition or imaging, are also potentially helpful in the search for micron- or nanometre-scale magnetic alloys such as awaruite. For example, Bina and Henry (1990) measured the magnetic properties and Curie temperatures of sixteen harzburgites from the Kane Fracture Zone on the Mid-Atlantic Ridge (Ocean Discovery Program (ODP) hole 670A). Their results are consistent with the absence of native metals such as awaruite in these samples, and with the findings of EPMA data and whole-rock metal concentrations.

Transmission electron microscopy (TEM), which permits nanometre-scale spatial resolution, has been used to characterize tiny alloy phases from terrestrial and extra-terrestrial samples (e.g., Jimenez-Franco et al., 2020), but preparation is time-consuming and quantitative analysis can be challenging. More recently, atom probe tomography (APT) has been used to characterize alloys (Daly et al., 2017; Evans et al. in press; Parman et al., 2015), and this technique offers quantitative analysis, including some isotope ratios, once the lengthy preparation, which involves extraction and milling of the sample to be analysed using a focussed ion beam (FIB), has been completed. APT has revealed previously unknown levels of complexity within alloy grains (Fig. 1), and interpretation of these features enables new constraints to be placed on the genesis and evolution of alloys hosted by ultramafic rocks.

3. Alloy-forming and modifying environments in ultramafic rocks

Distinctive PGM assemblages occur within ultramafic rocks from different tectonic settings, including layered intrusions, ophiolites from a range of geodynamic settings (e.g., O'Driscoll and Gonzalez-Jimenez, 2016), supra-subduction zone upper mantle, where alloys are commonly hosted by chromitite and pyroxenite (e.g., Becker and Dale, 2016), abyssal serpentinites, rodingites, subducted serpentinites, and serpentinites that have undergone contact metamorphism. Ancient refractory alloys and alloys formed within Earth's mantle may be altered by hydrothermal, metamorphic, or weathering processes (e.g., Hanley et al., 2005). Awaruite-bearing assemblages are summarized in Table 1, and similar details for the PGE-bearing alloys are provided by O'Driscoll and Gonzalez-Jimenez (2016).

3.1. Serpentinisation

Awaruite is a relatively common product of serpentinisation, and the PGMs may also form alloys by desulfidation during serpentinisation within a range of serpentinising environments that are discussed separately here. There is inevitably some overlap between the categories because serpentinised rocks have commonly undergone serpentinisation in more than one environment. To deal with this, we have attributed the consequences of serpentinisation to the dominant environment, so far as possible, with the proviso that some features may reflect prior or overprinting serpentinisation.

3.2. Abyssal serpentinites

The majority of reported alloys within abyssal serpentinites are awaruite or PGE-bearing alloys, but other alloys are reported, including native Au, Cu, and Cu–Ni–Fe alloys (e.g., Schwarzenbach et al., 2014). Awaruite typically coexists with a range of minerals that record low fS_2 and $aSiO_2$, elevated fH_2, and a range of aH_2O values. These phases include a range of combinations of ferroan brucite, lizardite, chrysotile, magnetite, pentlandite, heazlewoodite, and hydroandradite (e.g., Alt and Shanks, 1998; Evans and Frost, 2021; Frost, 1985; Horita and Berndt, 1999; Klein et al., 2009; Klein and Bach, 2009; Peretti et al., 1992).

For example, serpentinised harzburgites from the Samail Ophiolite, Oman, host awaruite and ferroan brucite that replace olivine (Rajendran and Nasir, 2014), and show an association with veins bearing hydroandradite garnet (Templeton et al., 2021). In contrast, awaruite within brucite-bearing partly serpentinised rocks from the 15′20"N Fracture Zone on the Mid-Atlantic Ridge is associated with magnetite and pentlandite within weakly serpentinised rocks that show evidence of desulfidation (Klein and Bach, 2009). In these rocks, increasing serpentinisation led to the loss of awaruite and formation of heazlewoodite–magnetite–pentlandite and millerite–polydymite–pyrite assemblages.

Awaruite from the Santa Elena ophiolite, Costa Rica, coexists with pentlandite, magnetite and a range of Cu-bearing phases, including native Cu. Here awaruite occurs even in completely serpentinised rocks, in contrast to the majority of occurrences where awaruite is only present during the initial phases of serpentinisation (Schwarzenbach et al., 2014). Native Cu and other Cu-bearing alloys are thought to have formed after the breakdown of pentlandite to form awaruite and magnetite, based on textural evidence that includes the replacement of awaruite by the Cu-bearing alloys. This textural relation places the introduction of Cu by hydrothermal fluids at moderate temperatures (350–400 °C), potentially similar to those of black smokers elsewhere on the seafloor, after the low-temperature serpentinisation (200–250 °C) recorded by awaruite.

The persistence of awaruite within the Santa Elena rocks is attributed to the formation of the system within the lower parts of the ocean crust, where direct interaction between the rocks and seawater was not possible. Instead, hydrothermal fluids were strongly modified by interaction with rocks on earlier stages of their flow paths, and limited infiltration resulted in low instantaneous water:rock ratios. Both of these factors facilitated retention of awaruite.

Similarly, awaruite is retained, even at high degrees of serpentinisation, within serpentinites from Site 1068, Ocean Drilling Program (ODP) Leg 173, Iberian abyssal plain, where serpentinites are separated from overlying sedimentary and tectonic breccias by a fault contact (Beard and Hopkinson, 2000). Awaruite occurs with pentlandite, heazlewoodite, and serpentine, even within strongly serpentinised rocks, and commonly coexists with andradite. In rocks close to the fault

contact, awaruite is replaced by tochilinite, pyrite, marcasite, and a range of other S-rich minerals. The persistence of awaruite is attributed to highly reduced serpentinising fluids formed by equilibration with other serpentinising rocks (Beard and Hopkinson, 2000).

3.3. Ultramafic intrusions

Mafic and ultramafic intrusions host some of the world's largest PGE resources, so the distribution of alloys within PGE-rich bodies, and the effects of serpentinisation, have been documented in some detail. For example, serpentinisation of the Dumont Sill, Abitibi, Quebec, Canada, which is a zoned intrusive body that includes lower ultramafic rocks, a mafic zone, gabbros, and quartz gabbros, formed awaruite and heazlewoodite within serpentinised dunites at the expense of Ni-bearing olivine in sulfide-poor rocks (Eckstrand, 1975; Sciortino et al., 2015). Here, Ni is thought to have been derived only from Ni-bearing silicates, and low water–rock ratios, low $a\mathrm{SiO_2}$, and low $a\mathrm{H_2O}$ facilitated awaruite formation. Awaruite did not form where magmatic sulfides provided a source of S. The early stages of serpentinisation formed Fe^{3+}-rich serpentine and Fe-rich brucite, whereas the later stages of serpentinisation formed Mg-rich serpentine, brucite, and abundant magnetite. Awaruite remained stable throughout serpentinisation, such that the highest modes of awaruite are found within completely serpentinised rocks (Sciortino et al., 2015).

Dunitic units may also occur within concentrically-zoned Uralian-Alaskan-Aldan-type complexes (CUAAC). These intrusions commonly show concentric zoning from a dunite-rich core to a gabbroic envelope via some combination of pyroxenites, wehrlites, hornblendites, and magnetitites (e.g., Johan, 2002). During serpentinisation, Pt-Fe alloys from CUAAC deposits commonly develop rims of Cu-bearing alloys or alter to S- and As-bearing PGMs, PGE-alloys, and awaruite within altered parts of the Matysken CUAAC, Koryak Highlands, eastern Russia. Here, Pt-Fe alloys are associated with hydrous silicate alteration and occur within the chlorite matrix, where they form isoferroplatinum–amphibole intergrowths. These alloys coexist with a range of other PGE-, Fe-, and Cu-bearing alloys, as well as S-, As-, and Sb-bearing PGMs, and provide evidence of PGE mobility and the stability of isoferroplatinum during serpentinisation (Kutyrev et al., 2021).

3.4. Chromitites from a range of geodynamic settings

Serpentinised chromitites are commonly rich in awaruite and PGMs, including PGE-alloys. Chromitites are found within ultramafic rocks from a range of geodynamic settings, but the assemblages and textural features relate more closely to the host rock type and serpentinisation process than the specific geodynamic setting, so they are grouped together here.

Serpentinisation does not always cause recognisable changes to the PGE distribution or PGM assemblage of chromitites. Chromitites of the Orhaneli and Harmancik ophiolites (Bursa, NW Turkey) do not show any secondary PGMs within the secondary silicate groundmass, which hosts bornite, awaruite, heazlewoodite, and violarite (Uysal et al., 2015). However, in many other occurrences, there is convincing evidence of low-temperature alloy formation and differential mobility of the PGEs on at least the small-scale. For example, secondary PGE-alloys that coexist with Pt-bearing awaruite, Ru-pentlandite, millerite, and PGE-bearing arsenides, oxides, and antimonides within chromitites from the At 'Ays ophiolite complex, Saudi Arabia show little evidence of large scale mobility of the PGEs, but evidence of small-scale mobility is provided by Pt stringers within altered silicates and the presence of PGMs within magnetite-filled veins that cut chromite (Prichard et al., 2008). In addition, remobilization of PGEs during serpentinisation of chromitites from southern New South Wales, Australia, is required to explain the formation of a secondary assemblage of native Au, Ru, Pd, and awaruite with millerite, heazlewoodite, polydymite, chalcopyrite, trevorite, magnetite, pentlandite, serpentine, and uvarovite garnet from a primary assemblage of PGE-bearing Ni-sulfides (Franklin et al., 1992; Graham et al., 1996).

Alloys, including awaruite, within chromitites are commonly interpreted to record low temperature desulfidation of a higher-temperature assemblage. Examples include the following:

- Chromitites of the Advocate ophiolite complex, Baie Verte Peninsula, Newfoundland, Canada, host Pd-group PGEs + base-metal alloys in association with ferrit-chromite, Fe-oxides, serpentine, chlorite, awaruite, heazlewoodite, and Co-rich pentlandite, which are inferred to have formed during serpentinisation (Escayola et al., 2011). Ir-group PGE-alloys from the same area are interpreted to have a magmatic origin.
- Ru-alloys and awaruite within cracks hosted by Ru-rich pentlandite from chromitites of the Vourinous Complex, north-western Greece (Garuti and Zaccarini, 1997).
- Awaruite rims on pentlandite coexisting with secondary silicates, bornite, heazlewoodite, violarite, and orcelite within chromitites from the Orhaneli and Harmancik ophiolites, Bursa, northwest Turkey (Uysal et al., 2015);
- Formation of Os–Ir–Ru alloys by desulfidation of laurite from chromitites of the At 'Ays ophiolite complex, Saudi Arabia (Prichard et al., 2008).
- Formation of Os–Ir–Ru alloys by desulfidation of laurite within podiform chromitites from Veria, Greece (Tsoupas and Economou-Eliopoulos, 2021). Here, the alloys coexist with awaruite, heazlewoodite, undescribed carbon-bearing material, and oxides that are associated with ferrit-chromite and andradite-uvavorite garnets

The low $f\mathrm{S_2}$ required for desulfidation of existing PGMs and BMS is commonly invoked as necessary for awaruite formation. For example, awaruite that co-exists with brucite, chlorite, apatite, calcite, heazlewoodite, and chalcocite within altered podiform chromites from the Hegenshan ophiolitic complex, Inner Mongolia, China (Jiang and Zhu, 2020), is inferred to have formed at lower $f\mathrm{S_2}$ than awaruite-free assemblages from the same area.

Serpentinisation-related modification of PGMs and alloy formation may be superimposed upon earlier hydrothermal alteration. For example, the hydrothermally-altered chromitites from Ouen Island, New Caledonia described by Gonzalez-Jimenez et al. (2011) record growth of new Pt–Pd–Rh–BM alloys and oxides, including awaruite, and continued stability of Pt-Fe alloys, although Pt-Fe alloys associated with chlorite and ferrit-chromite show high Pd contents, consistent with Pd mobility during alteration.

3.5. Suture zone ophiolites

Ultramafic rocks commonly occur within ophiolites hosted by alpine-type suture zones, where ophiolitic slivers occur within intensely-deformed linear belts that separate areas of different tectonic affinity.

The Baptiste Deposit, which is hosted by the Cache Creek Formation, British Columbia, which hosts an economic resource of awaruite-hosted Ni-mineralisation (Britten, 2017) is one such example, and includes ophiolites derived from supra-subduction and fore-arc mantle on the over-riding plate, and oceanic crust associated with a seamount oceanic plateau on the subducting plate. In this area, awaruite is hosted by units that were serpentinised and sheared during regional metamorphism. The fluid source is thought to have been meteoric water.

Awaruite within the Baptiste Deposit coexists with magnetite or forms rims on pentlandite and heazlewoodite. High resolution mapping of samples from Atlin, another locality within the Cache Creek Terrane, by LA–ICP–MS revealed that awaruite coexists with clusters of micron- and nanometre-scale PGM, tellurides, bismuthides, and other metal alloys (Lawley et al., 2020). Awaruite grains in this area reach several hundred microns in size, much larger than the awaruite typically found within abyssal serpentinites. The size difference is attributed to

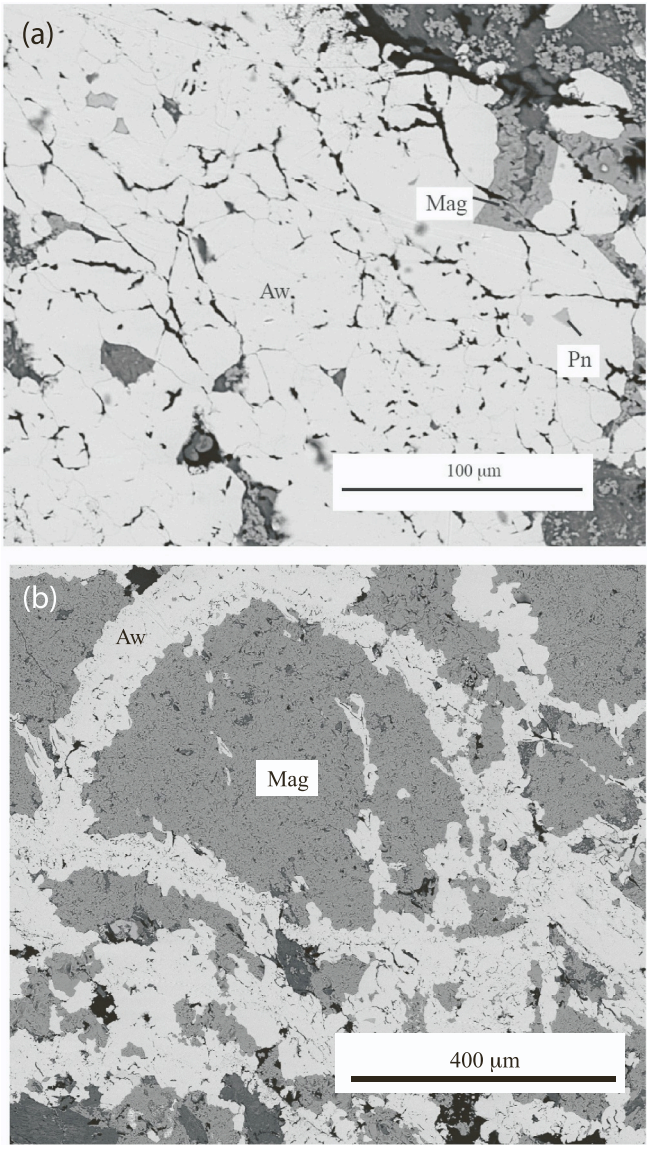

Fig. 2. BSE images from a single nugget of josephinite. A. Awaruite with small inclusions of pentlandite (Pn) and magnetite (Mag). B. Veins of awaruite (Aw) cutting magnetite (Mag). Sample courtesy of Henry Dick.

recrystallisation at elevated temperature (>300 °C) during regional metamorphism, based on the correlation between grain size and serpentinisation temperature. The growth of large awaruite grains is also favoured by the low S content of these rocks (200–400 ppm), which is similar to the average S content of the upper mantle (300–400 ppm), and lower than that of many serpentinites (200–16,000 ppm; Paulick and Bach (2006). The low S content reduces the probability of sulfide formation in response to the release of Fe from serpentinising olivine and is a common feature in alpine ultramafic rocks that are prospective for economic awaruite mineralisation. Other factors that favour abundant large awaruite grains are the relatively small water:rock ratios (see below for discussion), and prolonged strain related to accretion and later shearing, which increases the likelihood of pervasive, rather than focussed, fluid flow.

Another example is provided by partially serpentinised peridotites from the Chimaera seeps, Turkey, where awaruite coexists with millerite, heazlewoodite, Cu-bearing sulfides, native Cu, and S-poor, methane and H_2-rich fluids, is thought to form by desulfidation of primary pentlandite (Schwarzenbach et al., 2021). The Chimaera seeps occur within an actively serpentinising continental environment, but awaruite formation is thought to have occurred in an abyssal setting, based on the S isotope compositions of the serpentinisation products.

A relatively unusual association occurs within ultramafic rocks within ophiolites of the Ospa-Kitoi region, East Sayan, Siberia. Here, awaruite coexists with carbon-bearing phases that range in crystallinity from amorphous carbon to graphite (Zhmodik et al., 2004), and PGMs, Au, sulfides, arsenides, and sulfates (Airiyants et al., 2022). Awaruite is commonly intergrown with PGE-alloys, and the association is attributed to desulfidation of PGM-rich rocks during serpentinisation.

Another unusual association is that of Fe-bearing monticellite ($CaMgSiO_4$) that hosts awaruite inclusions, a few microns across, within the Happo Ultramafic Complex, Japan (Nozaka, 2020). Tiny magnetite grains are also present. This association is thought to have formed during static serpentinisation and Ca-metasomatism at 300–350 °C, and awaruite inclusions are interpreted to have formed to accommodate Ni that was released by olivine breakdown.

3.6. *Supra-subduction zone mantle*

Supra-subduction zone mantle is usually sampled after it has been obducted as part of an ophiolite, and serpentinisation within these rocks may have occurred in response to infiltration of fluids from the downgoing slab, during obduction, or by interaction with meteoric fluids in a continental setting. These complexities present challenges in attribution of the formation of serpentinisation-related alloys to any particular process, but some common features and processes are observed.

Some of the coarsest examples of native alloys are those associated with josephinite. Although a few in situ occurrences are recorded, josephinite occurs mostly as nuggets in a few creeks cutting the Josephine peridotite in the Cascade Mountains of SW Oregon (Dick, 1974), where it is likely to have been obducted from a supra-subduction zone setting. Josephinite nuggets range in weight from grams to nearly 50 kg (Dick, 1974; Jamieson, 1905). Technically, josephinite is a rock type because the nuggets consist of an assortment of Fe-Ni alloys, magnetite, sulfides and silicates (Botto and Morrison, 1976). The major mineral in josephinite is awaruite, but, because of the abundance of other phases are present in josephinite, it is incorrect to consider awaruite and josephinite as synonyms. Botto and Morrison (1976) noted that some occurrences of josephinite contain two Fe-Ni alloys; awaruite, which is roughly $FeNi_3$ and taenite, which is more iron-rich. Because the stability field of taenite relative to awaruite decreases with increasing temperature, Botto and Morrison (1976) concluded that josephinite formed over a temperature range of 350–450 °C. They concluded that nuggets bearing awaruite and taenite formed at relatively high temperatures, whereas those with only awaruite formed at lower temperatures.

In addition to Fe-Ni alloys, josephinite nuggets may also contain wairauite (FeCo), native copper, native silver and gold (Botto and Morrison, 1976; Dick, 1974). Silicate minerals include andradite, diopside, and serpentine. Magnetite occurs within the awaruite-rich samples (Botto and Morrison, 1976, Fig. 2). Ramdohr (1950) recognised numerous sulfides in josephinite, including pyrrhotite, heazlewoodite, chalcopyrite, chalcocite and sphalerite and Bonazzi and Bindi (2021) and Kakefuda et al. (2020) report the coexistence of awaruite with Ni-arsenides.

The size of the josephinite nuggets is extraordinary relative to the size of most awaruite grains, and is difficult to explain without transport of Fe and Ni, in contrast to most awaruite occurrences, which are consistent with isochemical serpentinisation. Dick (1974) observed that the streams that contain josephinite follow serpentinised shear zones that cut the Josephine peridotite. He concluded that the josephinite formed as part of the serpentinisation process and postulated that the coarse grain size might be related to metasomatism related to the intrusion of mafic dikes that occur within the area.

Elsewhere, PGEs show evidence of mobility during serpentinisation of supra-subduction zone mantle. In Jamaica, native copper from an ophiolitic section that crops out within the Blue Mountains east of

Kingston hosts substantial concentrations of Pt and Pd, of up to 23 and 15 wt% respectively (Scott et al., 1999), although the grains are tiny (0.25–0.5 μm), so the host of the PGEs could not be identified unambiguously. Similarly, Pt-bearing awaruite coexists with pentlandite, heazlewoodite, native copper, magnetite, millerite, and PGMs within partly serpentinised harzburgites from the New Caledonia ophiolite (Auge et al., 1999; Evans et al., 2017). In these rocks serpentinisation is thought to have mobilised Pt from primary base-metal sulfides into awaruite at temperatures of <400 °C.

Native Cu occurs within some supra-subduction zone serpentinites. For example, native Cu coexists with awaruite, magnetite, ferritchromite, heazlewoodite and pentlandite within the Dun Mountain Ophiolite Belt, New Zealand (Brathwaite et al., 2017). Chromite compositions are consistent with a supra-subduction zone origin for this dunite, and serpentinisation is thought to have been facilitated by infiltration of seawater into mantle peridotite along detachment faults.

Alloys formed within supra-subduction settings may survive subsequent changes to the geological setting. For example, awaruite occurs with heazlewoodite and magnetite within partly serpentinised peridotites from the La Cabana area, south-central Chile, that have been subducted and exhumed (Gonzalez-Jimenez et al., 2021). The awaruite–heazlewoodite–magnetite assemblage is interpreted to have formed in equilibrium with lizardite within supra-subduction zone mantle, before incorporation of the rock into the subduction channel (Gonzalez-Jimenez et al., 2021).

3.7. Subducted serpentinites

Awaruite is not commonly reported from subducted and exhumed serpentinites. However, serpentinites from the La Cabana area, south-central Chile, host awaruite with magnetite and heazlewoodite (Gonzalez-Jimenez et al., 2021). The Ni-rich phases are thought to have formed by desulfidation of pentlandite within a supra-subduction zone setting prior to subduction (see above). Infiltration of S-, As-, and Sb-bearing fluids within the subduction channel has overprinted the awaruite-bearing assemblage with S-rich phases such as millerite and As-rich phases such as orcelite and maucherite. The PGE contents of awaruite are low, which is interpreted to reflect mobility of the PGEs under high *P*–*T* conditions.

Tiny grains of Ni-rich awaruite (Ni_5Fe) are recorded in two samples from the Orocopia Schist, southwest Arizona, USA, which is interpreted as an exhumed subduction channel (Haxel et al., 2018). The textural details are not reported, but pentlandite, cobalt pentlandite, heazlewoodite, occur with orcelite, maucherite, and rare pyrrhotite, bornite, and bismuthinite. These assemblages demonstrate the capacity of S- and As-bearing fluids or bulk compositions to stabilise other minerals relative to awaruite, and it is likely that awaruite within ultramafic rocks from most subduction channel settings is relict and records a previous stage of the rock's evolution.

3.8. Contact metamorphism

Awaruite is rarely reported from contact-metamorphosed ultramafic rocks, but is documented to coexist with magnetite, heazlewoodite and pentlandite within the metamorphic aureole of a granite that intrudes an ophiolite that has been incorporated into a Palaeozoic accretionary complex in the Chugoku District, southwest Japan (Nozaka, 2003). In these rocks, awaruite co-exists with magnetite far from the intrusion and its mode decreases with increasing proximity to the intrusion as the modes of magnetite, pentlandite, and heazlewoodite increase. This is consistent with destruction of awaruite within contact metamorphic settings by high temperature metamorphism and the presence of water-rich intrusion-derived fluids.

3.9. Weathering

While magmatic temperatures favour ordered stoichiometric alloy compositions, the compositions and structures of alloys formed in weathering environments are likely to be controlled by the local availability of alloy components under transport-limited conditions, so less-ordered alloys that may be metastable might form (e.g., Bowles et al., 2017), or oxides and hydroxides, which are not discussed further here (e.g., Cabral et al., 2008). Iron- and Ni-bearing alloys may not persist over long timescales in weathering environments, but there are few descriptions of changes to the composition and morphology of Fe-Ni alloys from weathering environments. However, Challis (1975) reports an increase in the Ni-content of alloy flakes found in stream sediments of the Jerry River, South Westland, New Zealand, as a function of distance from the assumed source, which is the Red Hills Range.

In contrast, PGE alloys are observed in weathered rocks (e.g., Bowles et al., 2017), and some of the PGEs are mobile in the weathering environment. For example, Fuchs and Rose (1974) and Wood (1991) inferred that Pd and Au are mobile in surface environments relative to Pt, and Bowles et al. (1994) showed that organic acids can complex with Pt and Pd at 25 °C.

Weathering of PGE minerals and transport of PGEs within the weathering environment are evident in tropical environments such as those found on the Freetown Peninsula, Sierra Leone. Here, the primary hosts of Pt-bearing alloys are magnetite-bearing gabbros that contain PGE mineralisation associated with Ni-poor and Cu-rich sulfides (Bowles et al., 2013), and weather to form alluvial deposits related to intense weathering and saprolite formation (Bowles et al., 2017). At this location, it is possible to study the effects of intense tropical chemical weathering on PGMs.

In the source rocks, the PGMs form grains, <10 μm in size, that typically form inclusions within the silicates and sulfides. The PGMs are much less common within the gibbsite-dominated saprolite, although rutile, zircon, and other highly resistant minerals are preserved. Of 97 grains documented by Bowles et al. (2017) the majority are Pt-Fe alloys with compositions ranging from Pt_3Fe to PtFe, and cooperite (PtS). A smaller proportion show detectable Cu concentrations. Laurite (RuS_2), malanite ($CuPt_2S_4$) and a Rh-rich sulfide are also present.

Weathering decreases the S content and size of the alloys, increases the degree of disordering, increases Fe:Pt values and Cu-content, and increases the proportion of composite grains comprising Pt–Fe ± Cu alloys, which are commonly surrounded by Fe- and Al-hydroxides. Copper is thought to be mobilised from Cu-sulfides to form composite Cu-bearing PGM grains. Alteration of Pt-bearing minerals is demonstrated by the formation of filamentous Pt-rich material within sulfides, mottling within weathered cooperite, and the formation of composite PGM grains. A substantial proportion of the PGEs evident from bulk rock compositions are not accounted for by the PGM grains, indicating that some PGEs are "invisible", most likely as adsorbed Pt and Pd on secondary minerals to form oxides, hydroxides, and organometallic compounds. Further, changes in whole-rock Pt:Pd values indicate transport of the PGEs within the weathering environment.

4. Quantitative constraints on alloy-forming environments

Quantitative estimates of the relative stabilities of minerals within the system Fe–Ni–O–S ± Co ± H ± Si ± Mg have been presented by a number of studies (e.g., Eckstrand, 1975; Evans et al., 2017; Foustoukos et al., 2015; Frost, 1985; Frost et al., 2008; Frost et al., 2013; Klein and Bach, 2009). For example, thermodynamic data for minerals within the system Fe–Ni–Co–O–S were compiled by (Klein and Bach, 2009), and phase relations were calculated for temperatures ranging from 150 °C to 400 °C and 50 MPa as a function of fO_2, fS_2, fH_2, and fH_2S.

These calculations are based on the principles of equilibrium thermodynamics, so the assumption of thermodynamic equilibrium is implicit in their use. Thermodynamic equilibrium within serpentinites at

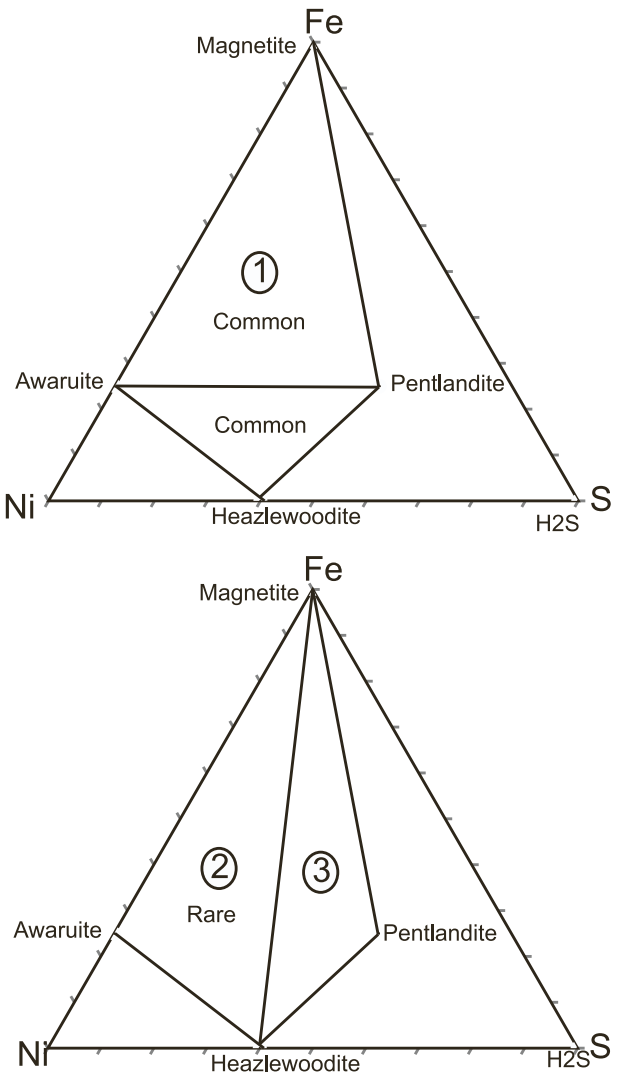

Fig. 3. Fe–Ni–S ternary diagrams showing common awaruite-bearing assemblages summarized in Table 1.

the temperatures of awaruite formation is on limited length scales, based on the observation that assemblages can vary on the millimetre scale between, for example, originally olivine- or orthopyroxene-dominated domains, and the composition of serpentine veins can vary on the length scale of a few tens of microns (e.g., Evans et al., 2013; Frost et al., 2013). The length scale of equilibrium for PGEs may be shorter than the distance between grains (Evans et al. in press). Nevertheless, mineral assemblages and textural relationships within a domain are generally relatively consistent, so it is reasonable to assume that the systems were at, or close to, thermodynamic equilibrium and that they can be interpreted on this basis so long as length scale limitations are carefully observed and considered.

There is consensus that awaruite formation during serpentinisation occurs under conditions of low $a\mathrm{SiO_2}$, $f\mathrm{S_2}$ (or $a\mathrm{H_2S}$), and high $f\mathrm{H_2}$, which corresponds to low $f\mathrm{O_2}$, because $f\mathrm{H_2}$ and $f\mathrm{O_2}$ are linked by the expression for water decomposition ($\mathrm{H_2O = H_2 + 1/2O_2}$) (e.g., Eckstrand, 1975; Foustoukos et al., 2015; Frost, 1985; Klein and Bach, 2009; Sciortino et al., 2015). These parameters are mostly buffered by the mineral assemblages, based on the relatively high number of phases in most awaruite-bearing serpentinites (Table 1, Fig. 3). According to the phase rule, three coexisting solid phases plus a fluid within the system Fe–Ni–O–H–S constrain the assemblage to a line in $f\mathrm{O_2}$–$f\mathrm{H_2S}$ space at fixed pressure (P) and temperature (T), and four solid phases coexisting with a fluid within the same system buffer $f\mathrm{O_2}$–$f\mathrm{H_2S}$ to fixed values at a point in $f\mathrm{O_2}$–$f\mathrm{H_2S}$ (e.g., Fig. 4). For example, the concentration of $\mathrm{H_2S}$ is buffered by the awaruite-bearing opaque phase assemblages to around 1 mmol/kg at 350–400 °C and micromolar concentrations at 150–200 degrees C (Klein and Bach, 2009). The addition of components such as Co or Cu without the addition of another phase increases the field of stability for these three- and four-phase assemblages, but the assemblages would still be strongly rock-buffered while the additional components occur in trace concentrations. Similarly, co-existing brucite and serpentine or olivine and brucite buffer $a\mathrm{SiO_2}$ to 3–4 $\mathrm{Log_{10}}$ units below quartz saturation (Frost and Beard, 2007), even where limited solid solution with Fe-bearing end-members increases the variance of reactions.

The geometry of awaruite-bearing and adjacent fields does not vary much as a function of P and T (Fig. 4), but the absolute positions of lines and points vary with P, T, and the data selected for awaruite (Foustoukos et al., 2015), and partitioning and the oxidation state of Fe are sensitive to temperature and water:rock ratio during serpentinisation (Klein et al., 2009), which affects the relative stability of awaruite via the availability of electron donors and the stability of $\mathrm{H_2}$. For example, awaruite formation above 330 °C is less common than at lower temperatures because the $a\mathrm{H_2}$ required to stabilise this phase is higher than that provided by the mineral buffers; the assemblage awaruite + pentlandite + magnetite buffers $f\mathrm{H_2}$ to values close to the limit imposed by water stability at temperatures between 200 and 350 °C (Klein and Bach, 2009), although the awaruite stability field is extended if the data of Foustoukos et al. (2015) are used instead of that of Howald (2003). The maximum $f\mathrm{H_2}$ values predicted by Klein and Bach (2009) occur at 150 to 250 °C and water:rock ratios of 0.1 to 0.5, which is broadly consistent with the results of Sleep et al. (2004), who modelled co-existing $\mathrm{Fe^{2+}}$-bearing serpentine, brucite, magnetite and awaruite and inferred that Fe-rich serpentine ($X(\mathrm{Mg}) = 0.9$) coexists with awaruite at 100 °C and partial pressures of $\mathrm{H_2}$ of 10 to 20 MPa. However, the observations of Britten (2017) and Evans et al. (2017) indicate that awaruite can be stable within the antigorite stability field, consistent with the extended awaruite stability field predicted by Foustoukos et al. (2015), although this stability is likely to be much more limited than at lower temperature. Awaruite is most often observed within partially serpentinised rocks and becomes unstable relative to more S-rich assemblages with increasing serpentinisation (e.g., Evans et al., 2017), but awaruite has been observed, even in completely serpentinised rocks (e.g., Beard and Hopkinson, 2000; Ellison et al., 2021), and it has been proposed that its persistence might reflect ongoing serpentinisation driven by fluids that have equilibrated with serpentinites, so they remain reducing and S-poor.

5. Alloy-forming processes

The formation of metal alloys that may include Fe, Ni, Cu, Co, Pt, and Pd requires a source of metals in the alloy-forming environment and extremely low $f\mathrm{O_2}$ and $f\mathrm{S_2}$, which stabilise alloys in favour of sulfides and silicate hosts of the alloy-hosted metals.

These requirements are discussed here within the context of awaruite formation. Formation of PGE alloys requires similar environments to awaruite (e.g., Foustoukos et al., 2015), but they are challenging to interpret because they are formed and modified within a range of environments, they are typically tiny and easily missed during routine petrography, they can be hosted by a wide range of minerals because they can behave as trace or major elements within their hosting phases, and the thermodynamics of those minerals are not well known (but see Foustoukos et al., 2015, Foustoukos, 2019). Further, the low concentrations of the PGEs within most ultramafic rocks means that they provide excellent monitors of processes but are unlikely to provide strong controls on their environment; they can be viewed as responsive, rather than controlling, or, in other words, driven by bulk composition rather than affecting oxygen and sulfur fugacity. Similarly, Cu is a trace

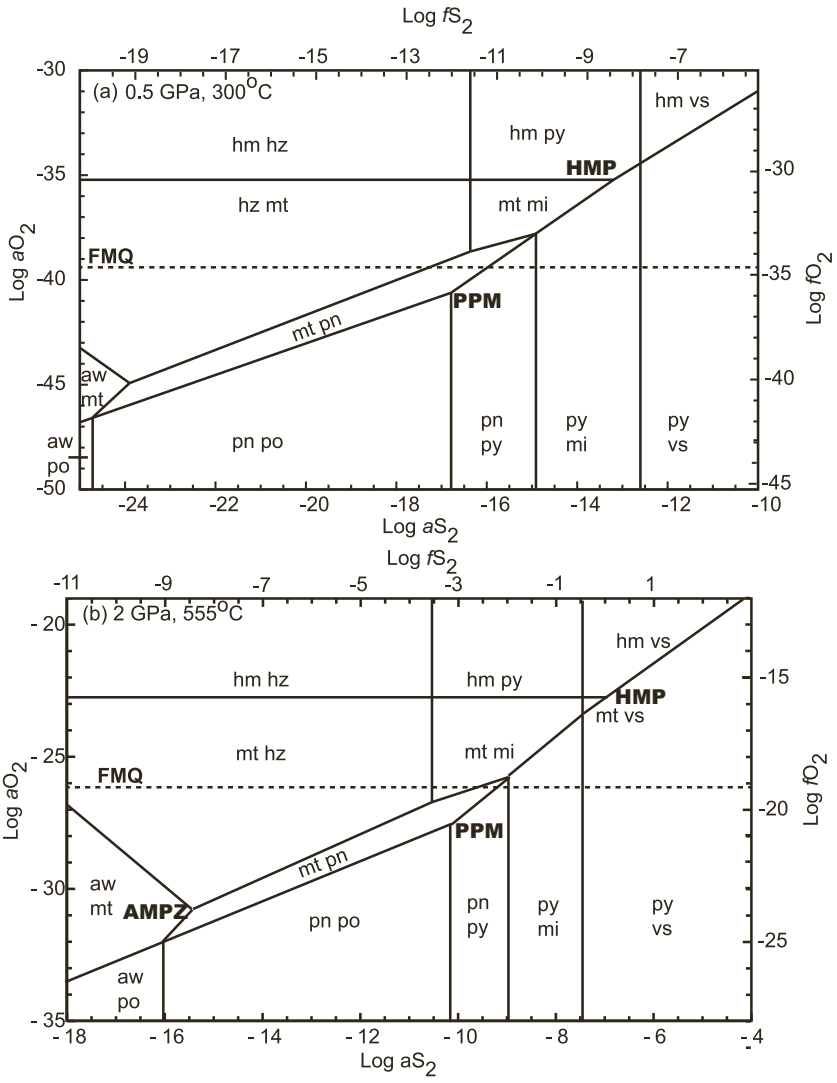

Fig. 4. Illustration of the distribution of stable sulfide and oxide assemblages within fO_2–fS_2 space at (a) 0.5 GPa and 300 °C; and (b) 2 GPa and 555 °C. Figures are adapted from those in Evans et al. (2017) and methods and data sources are provided within that article.

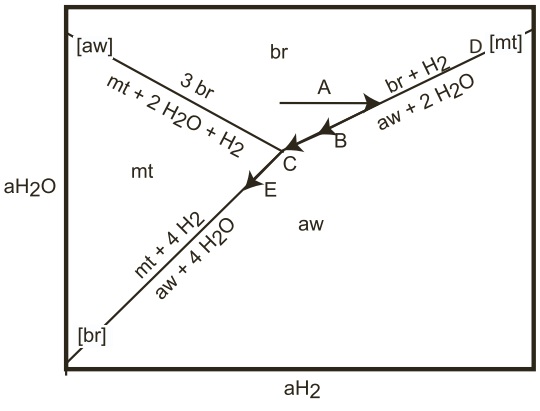

Fig. 5. Schreinemakers diagram showing the relative stabilities of native Fe (as a proxy for awaruite), Fe-brucite, and magnetite as a function of aH_2O and aH_2. The plot is schematic, but an upper temperature limit is provided by that of brucite-breakdown at 400–450 °C.

element within most peridotites and, while it has a wider stability field in fO_2 space than most alloys (Schwarzenbach et al., 2014), its stability is limited by fS_2, so an explanation of low fS_2 within serpentinites is also likely to explain the stability of native Cu.

In contrast, Fe is typically the most abundant redox-sensitive element within an ultramafic rock so the minerals it forms have the potential to control, as well as monitor, the redox conditions of the system. If we can understand the processes that produce an awaruite-forming environment then this understanding should be transferrable and provide insights into the formation of PGE-alloys and others, such as native Cu.

5.1. Sources of metals

Fe. An obvious source of iron in the alloys is the Fe^{2+} that is dissolved into olivine and other silicates and that is released during serpentinisation. X-ray images of serpentine veins in peridotite shows that Fe can be mobile during serpentinisation (Frost et al., 2013). It is also possible that the source of Fe can be magnetite or sulfides such as pyrrhotite and pentlandite.

Ni. There are two possible sources for Ni in alloys. One is from the silicates. Primary olivine in peridotite can contain up to 0.5 wt% NiO (Herzberg et al., 2016). In contrast, serpentine from serpentinised peridotites contains around 0.01% NiO, although serpentine from veins

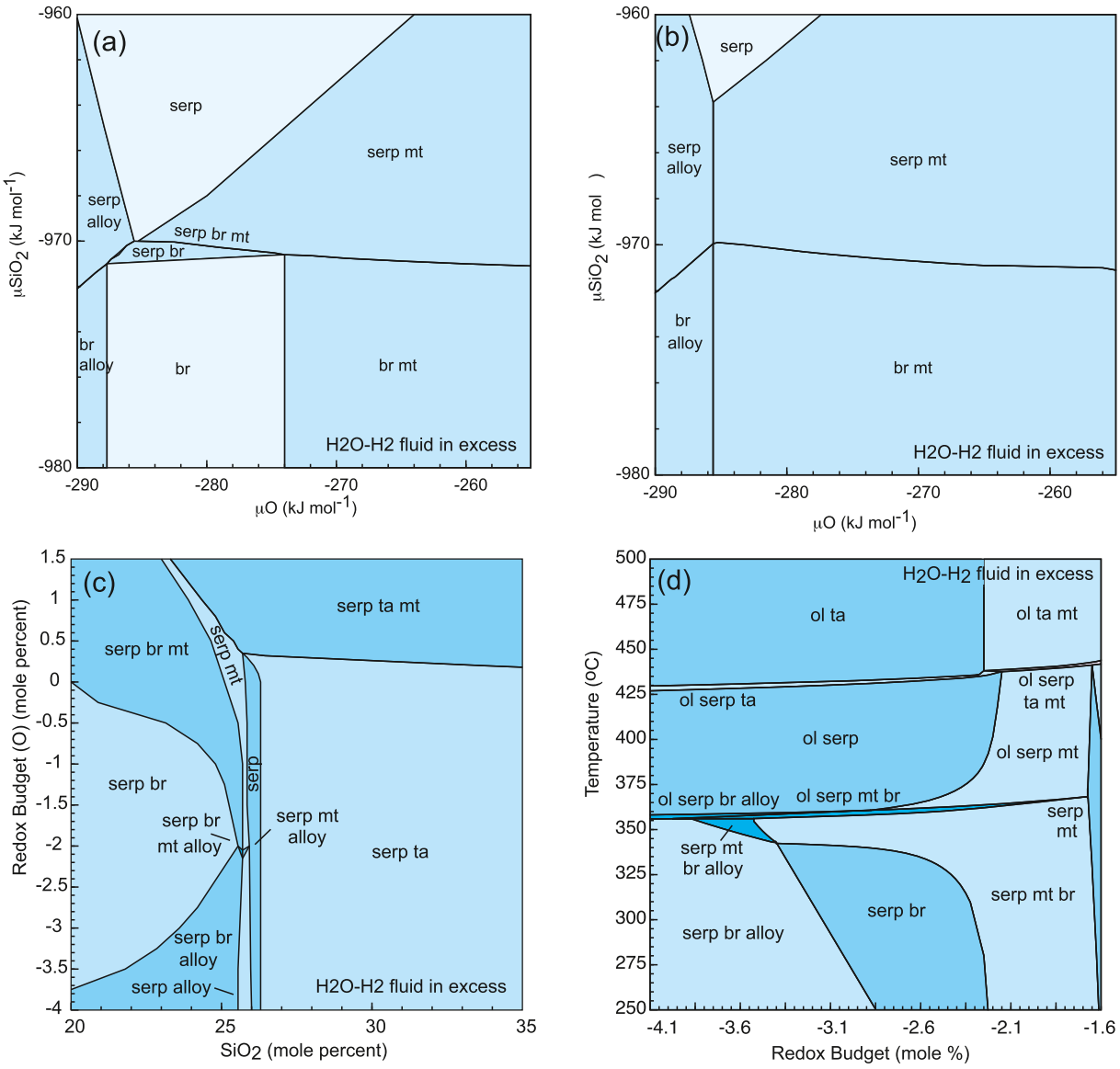

Fig. 6. Pseudosections within the system FMOSH at 0.1 GPa and 330 c, illustrating the sensitivity of alloy-bearing assemblage to: (a, b) μO_2 and μSiO_2 as a function of the system Mg/(Mg + Fe). Bulk composition taken from typical New Caledonia harzburgite. (a) $X(Mg) = 0.9$; (b) $X(Mg) = 0.7$; (c) Bulk system SiO_2 (mole %) versus bulk system O concentration (equivalent to redox budget, see Evans et al. (2013); (d) Redox budget versus temperature for a water-undersaturated system (molar H_2O:SiO_2:MgO:FeO = 40:23:33:5.4). Figures are adapted from those in Evans et al. (2013) and detailed methods are provided in that article.

contains around 0.2% NiO (Frost et al., 2013). This means that Ni may be lost from the silicates when serpentinisation takes place. Another possible source of Ni is pentlandite, which is a common sulfide in many peridotites and small amounts of Ni may be found within pyrite and pyrrhotite (Lorand, 1989).

Co. Like Ni, Co may be sourced from either olivine or pentlandite in the original peridotite. Because Co content of olivine is much lower than Ni (Herzberg et al., 2016), it is likely that Co in Fe alloys is sourced from protolith sulfides. Lorand (1989) found that primary monosulfide solid solution (MSS) or pentlandite in peridotite may contain up to 0.5% Co, whereas pyrite may contain nearly 2%. In contrast pyrrhotite typically contains <0.05% Co.

Cu. Copper within most ultramafic rocks is sourced entirely from sulfides. Lorand (1989) found that the major source of Cu in peridotites is chalcopyrite, although small amounts may occur in MSS. Pyrrhotite and pyrite contain only trace amounts (Lorand, 1989).

PGEs. Typical mantle values of the PGE are a few ppb, but peridotitic rocks from Alaska-type intrusions may contain up to 10 ppm PGEs that are mostly sourced in the chromite (Clark and Greenwood, 1972; Milidragovic et al., 2021). PGE-bearing chromitites also occur within ophiolites (Yurichev et al., 2021).

5.2. *Processes that form reducing, sulfur-poor fluids*

A range of processes has been proposed to explain the relationships amongst low fS_2, low fO_2, and low $aSiO_2$ during alloy formation and the textures that record these relationships. Suggested processes include fluctuating redox conditions (e.g., Graham et al., 1996; Tsoupas and Economou-Eliopoulos, 2021), an integral but loosely-connected role for brucite (e.g., Klein et al., 2009; Klein et al., 2014), and release of base-metals and PGEs during desulfidation of base-metal sulfides ((e.g., Foustoukos et al., 2015; Lawley et al., 2020). However, none of these provide a comprehensive explanation for a relatively small number of key observations that are common to most awaruite-bearing rocks. Ideally, the proposed process would be common to most awaruite-forming environments and involve elements that are present in sufficient concentrations that mass balance constraints for the formation of the observed H_2-rich fluids can be satisfied. The driving process may or

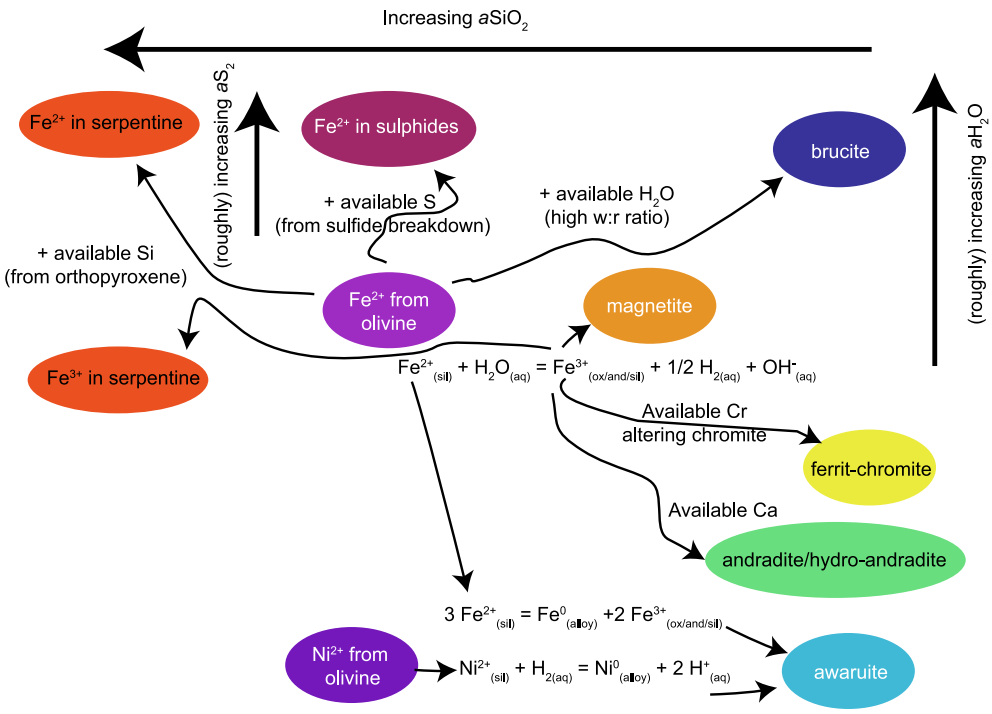

Fig. 7. Simplified illustration of the factors that influence the mineral hosts of Fe released by olivine serpentinisation and the relationships amongst them. The principal objective of the illustration is to show the complexity and the importance of multiple bulk compositional and external parameters that determine the mineral assemblage that forms during serpentinisation rather than to provide a complete quantitative description of the process. Transfer of electrons is shown as $H_2 = 2H^+ + e^-$, rather than by electrons directly, to reflect the paucity of electrons in solution.

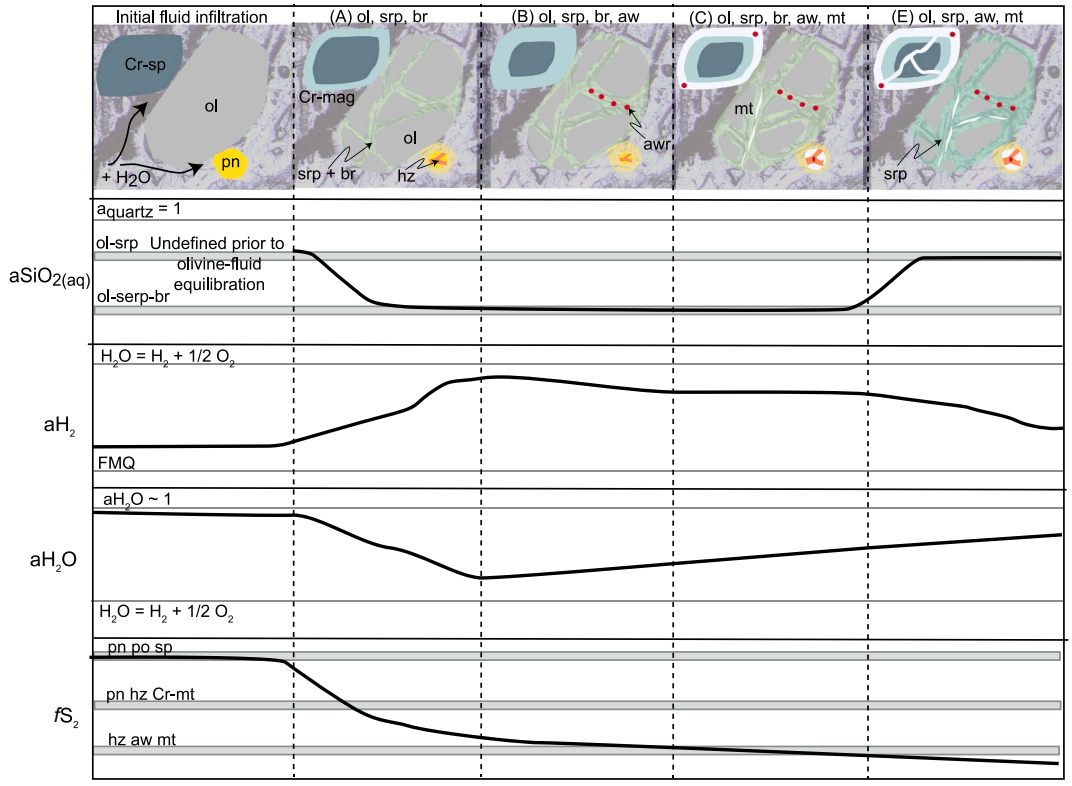

Fig. 8. Speculative conceptual model for early serpentinisation, showing the links amongst mineral assemblage and fluid composition parameters for olivine and serpentine with the following sequence of minerals: (A) brucite; (B) brucite + awaruite; (C) brucite + magnetite + awaruite; and (E) magnetite + awaruite. The labels refer to the regions on the Schreinemakers diagram in Fig. 5.

may not control $aSiO_2$ or fS_2 directly, and this is discussed below. Key observations include the following:

(1) The well-documented links between low fS_2, low fO_2 and low $aSiO_2$ (e.g., Frost, 1985; Frost et al., 2013; Klein et al., 2009; Klein and Bach, 2009).

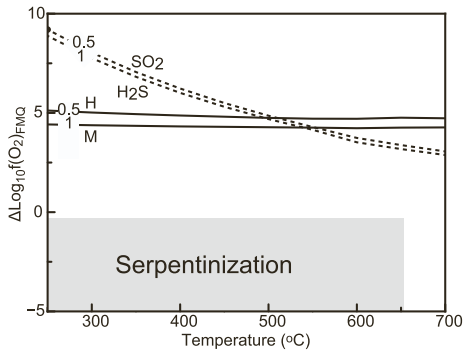

Fig. 9. Relationship between the SSO, hematite–magnetite (HM), and FMQ buffers as a function of temperature and pressure. Serpentinisation occurs within the stability field of H_2S. Labels indicate the pressure in GPa. Adapted from Evans and Frost (2021), and details of the calculations are provided there.

(2) Hydration of silicates leads to the formation of magnetite, destabilization of sulfides, and, in some cases, production of Fe-Ni or PGE alloys;
(3) The phase-rule, as discussed above, indicates that early serpentinisation, which is the alloy-forming phase, occurs under internally-buffered conditions.
(4) Early serpentinisation is isochemical on the cm scale, except for the addition of water (e.g., Frost et al., 2013).
(5) Brucite is commonly texturally early and can occur with or without magnetite and awaruite.
(6) Serpentinisation can proceed along different trajectories within fO_2–fS_2–$aSiO_2$–aH_2O–x(Mg) space, as shown by the range of different opaque-phase assemblages shown in Table 1 and documented by Eckstrand (1975). Alloy formation may occur early or not at all, and alloys may be destroyed by later serpentinisation (e.g., Evans et al., 2017) or persist even within fully serpentinised rocks (e.g., Beard and Hopkinson, 2000; Schwarzenbach et al., 2014). Similarly, sulfides may be destroyed, retained, or react to form S-rich sulfides such as violarite and polydymite (e.g., Graham et al., 1996; Klein and Bach, 2009), and $aSiO_2$ may be sufficiently low to form brucite, or sufficiently high to form talc (e.g., Paulick et al., 2006), although talc and alloys are not documented together with the exception of listvenites, which are not discussed further here.
(7) In many cases, alloys remain stable in serpentinites while olivine is present in the serpentinisation assemblage. In cases where alloys are retained after olivine depletion, it has been proposed that the fluid producing the serpentinisation was in equilibrium with olivine (Beard and Hopkinson, 2000). On destruction of alloys, the previously alloy-hosted metals may be transferred to magnetite or sulfides.
(8) Awaruite typically coexists with a phase that hosts Fe^{3+}. Most commonly this is magnetite, but one or more of andradite, hydroandradite, ferrit-chromite, Fe^{3+}-rich serpentine, and andradite–uvavorite garnet are also observed (e.g., Beard and Hopkinson, 2000; Evans et al., 2009; Templeton et al., 2021) and Table 1.

5.3. Conceptual model: a thought experiment

To understand the processes that lead to the low fS_2 and fO_2 that stabilise alloys, and the high fH_2, and low $aSiO_2$ values that accompany them, it is useful to consider the main driver or drivers of the complex suite of reactions that occur within serpentinites. By undertaking this task as a speculative thought experiment guided by the observations listed above, the causal relationships amongst these intensive parameters can be investigated, and correlation, causation, and parallel but otherwise unrelated consequences of the driving process or processes can be identified.

While it can be helpful to write simple reactions to relate the mineral and fluid endmembers, this can also, ultimately, be misleading, because element transfer between the phases is the integrated result of a set of independent reactions that occur simultaneously, and the reactants and products of the reactions, as written, may not be major species within the minerals or fluids (Evans et al., 2013). For example, dissolved O_2 makes frequent appearances within reactions written to explain the evolution of serpentinites but forms a vanishingly small proportion of the fluids that are present.

Olivine hydration is a process that satisfies the constraints and observations outlined above. It is common to alloy-forming environments and involves major elements. Serpentine, the most common product of olivine hydration, is typically more Mg-rich than the reacting olivine, so an Fe-bearing phase must form as a co-product of olivine hydration if the system remains isochemical except for H_2O and there is no local source of SiO_2. Serpentine is more SiO_2-rich, per metal cation, than olivine, so formation of serpentine from olivine within a closed system depletes the system in Si, decreasing $aSiO_2$ and favouring the formation of an Fe-rich product phase that is Si-poor or Si-absent. Common Fe-bearing phases that form as a consequence of olivine hydration are one or more of Fe-rich brucite, magnetite, ferrit-chromite, andradite, ferric-rich serpentine, and awaruite. In more Si-rich systems, the final products of serpentinisation are serpentine and magnetite (e.g., Syverson et al., 2017).

The Fe within Fe-rich brucite and olivine is dominantly or entirely Fe^{2+}, so the formation of brucite from olivine without olivine formation is not a redox reaction. This means that, while $aSiO_2$ is buffered to low levels by coexisting olivine and brucite (Frost and Beard, 2007), brucite formation alone does not lead to low fO_2 and no alloys are expected to form if brucite incorporates all of the excess Fe released by olivine. This is consistent with observations of brucite without awaruite or magnetite within a range of serpentinising systems (e.g., Frost et al., 2013).

Magnetite, andradite, ferrit-chromite, and Fe^{3+}-rich serpentine all contain Fe^{3+}, so their formation requires the transfer of electrons from Fe^{2+} derived from olivine to another phase. The most common electron acceptors within geological systems are Fe^{3+}, S^{-} to S^{6+}, and C^{4+}, but these elements are present in their more reduced forms (Fe^{2+}, S^{2-}, C^{-4}) within serpentinising peridotites prior to the formation of the Fe^{3+}-bearing minerals so they cannot act as an electron acceptor. Dissolved oxygen is also present within seawater, but at relatively low levels on the order of $\sim 10^{-4}$ mol l^{-1}, and its solubility decreases with increasing temperature, so it is likely to be consumed quickly during initial serpentinisation. In the absence of these solutes, the most likely electron acceptor is water-hosted H^+, which can accept electrons to form H_2 ($H^+ + e^- = 1/2H_2$), rock-sourced Fe^{2+}, which can form Fe^0 ($Fe^{2+} + 2\,e^- = Fe^0$), and rock-sourced Ni^{2+}, which can accept electrons to form metallic Ni within awaruite ($Ni^{2+} + 2\,e^- = Ni^0$). The redox budget consumed by Fe and Ni to form awaruite is typically much smaller than that required to explain the amount of Fe^{3+} in magnetite and other phases, because the amount of Ni is small relative to the amount of Fe. For this reason, in this conceptual model, H^+ is the main electron acceptor and production of H_2 drives the system towards low fO_2 via dissociation of water ($H_2O = H_2 + 1/2O_2$).

This progression can be observed within dunites from New Caledonia (Frost et al., 2013). Here, fluid flowing through fractures within serpentinised dunites during the earliest stages of serpentinisation produced Fe-enriched serpentine + brucite without magnetite, with X(Mg) values of 0.92 and 0.86 respectively. These are the Type I veins of Beard et al. (2009). Later, larger Type 2 and Type 3 veins contain magnetite and both the serpentine and brucite are relatively magnesian. In type 3 veins, the X(Mg) values of serpentine and brucite range up to 0.97 and 0.96 respectively.

It is then relevant to consider the factors that determine whether brucite or one of the Fe^{3+}-bearing minerals form during serpentinisation, and the causes of shifts between Fe-bearing products. During initial

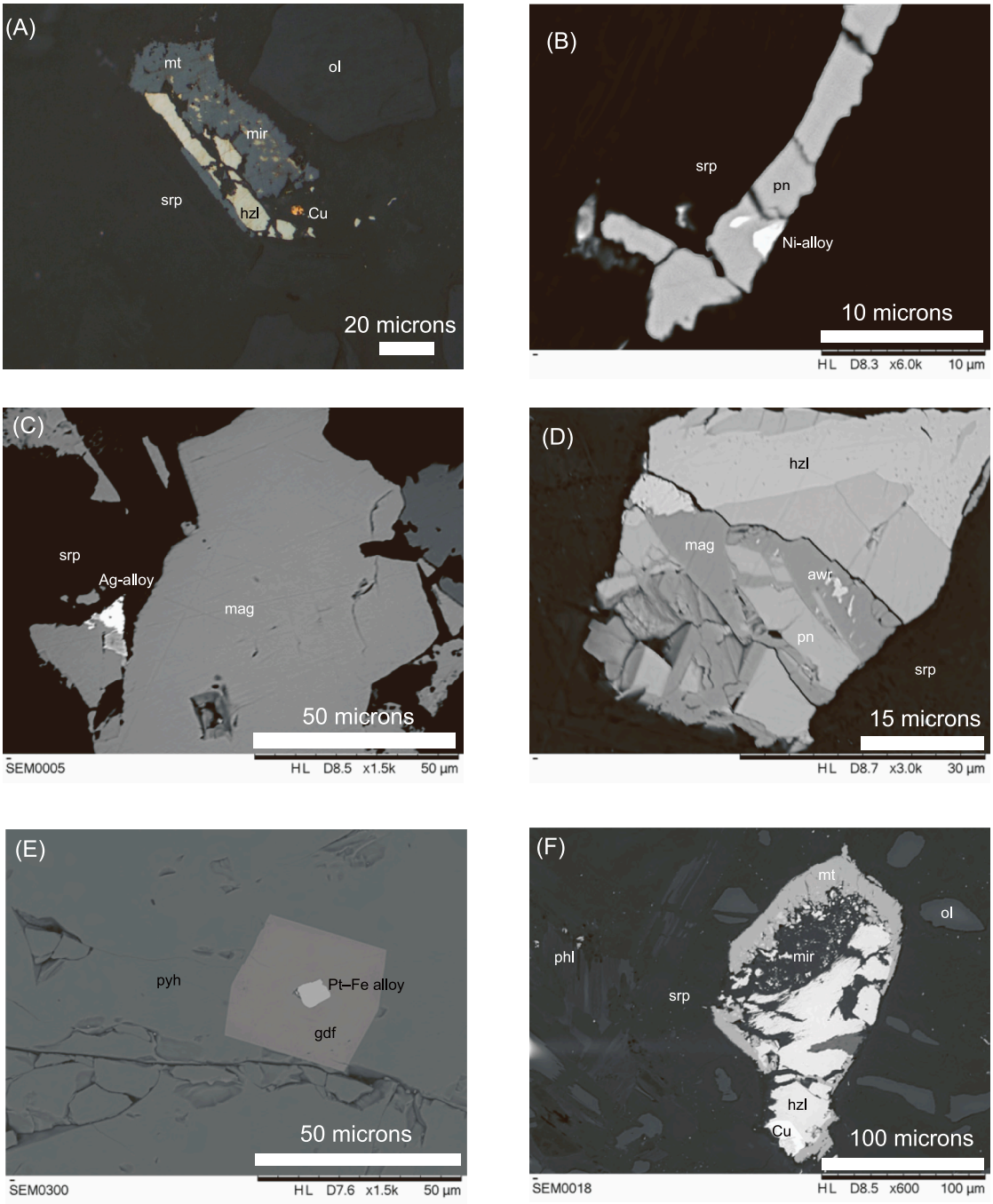

Fig. 10. Photomicrographs and back-scattered electron (BSE) images of serpentinites and partially serpentinised dunites from the Ta Khoa dome, Vietnam, showing some of the diverse range of assemblages and textures that record overprinting of awaruite-bearing assemblages by later sulfides and oxides. Sections are from the Ban Phuc ultramafic intrusion unless otherwise identified. (A) Native Cu associated with magnetite, heazlewoodite, millerite and apatite within a chlorite- and phlogopite-bearing partially serpentinised dunite. RFL, PPL, x50; (B) Ni-bearing alloy inclusion within pentlandite within phlogopite-bearing serpentinised dunite. This rock also hosts magnetite, heazlewoodite, and pentlandite. SEM-BSE; (C) Ag-rich alloy on the tip of a magnetite grain within a phlogopite- and chlorite-bearing, olivine-free, serpentinite. Other opaque phases include trace chalcopyrite, idaite, pentlandite, heazlewoodite, and bornite. SEM-BSE; (D) Awaruite inclusions within magnetite that forms part of a composite pentlandite–heazlewoodite–magnetite grain within a phlogopite-bearing serpentinised dunite. This section also hosts native Cu and pyrite. SEM-BSE; (E) Pt–Fe–As alloy inclusion with a gersdorffite rim hosted by pyrrhotite. Host rock is a semi-massive sulfide with silicate inclusions. Other opaque phases include pentlandite, chalcopyrite, ilmenite, magnetite, sphalerite, Pd-tellurides (King Snake prospect). SEM-BSE; (F) Native Cu associated with magnetite, heazlewoodite and millerite. Same rock as (A). SEM-BSE. Abbreviations on images are from Warr (2021). RFL: reflected light; PPL; plane-polarised light; SEM-BSE: scanning electron microscope back-scattered electron image.

serpentinisation, brucite is a common product, and this forms together with Fe-rich serpentine (Frost et al., 2013). The formation of brucite alone has no effect on fO_2, but studies of the speciation of Fe in serpentine indicate that the Fe^{2+} and Fe^{3+} contents of serpentine can be correlated (e.g., Evans et al., 2009; Sciortino et al., 2015). For example, Klein et al. (2009) measured Fe^{3+}/Fe_{tot} values of 0.3–0.5 for Fe within serpentine–brucite mesh rims on olivine from hole 1274A, which sampled the Mid-Atlantic Ridge at around 15° N, Seyfried et al. (2007) produced serpentine with Fe^{3+}/Fe_{tot} values of around 0.42 in experiments at 200 °C and 0.05 GPa, and a compilation of Mossbauer-derived

data (n = 68) shows Fe^{3+}/Fe_{tot} values ranging from 0.2 to 1 (Tutolo et al., 2020), although the proportion of these that coexist with awaruite was not documented. Evans et al. (2009) documented a broad range of X (Fe) values for lizardite; and a negative correlation between Fe and Si in lizardite, consistent with the findings of Tutolo et al. (2020), indicating that the Fe^{3+} content of lizardite increases with X(Fe) via a ferri-Tschermak's substitution to form a cronstedite component. The formation of the Fe^{3+} that is incorporated by serpentine requires an electron acceptor, which is most likely to be fluid-hosted H^+, so the H_2 content of the fluid would increase by this process, and the redox state of the system and H_2 production would be buffered by equilibria involving Fe^{3+}-bearing serpentine (e.g., Klein et al., 2014; Seyfried et al., 2007; Tutolo et al., 2020).

It is possible to investigate factors that relate to the formation of magnetite, brucite, and awaruite using a Schreinemakers' diagram to show the relative stabilities of these minerals within aH$_2$–aH$_2$O space (Fig. 5). Absolute values of the activities are not shown, but the slopes of the lines are determined by the stoichiometry of the reactions. Sulfur is omitted, based on the assumption that it is controlled by, rather than controlling, the redox conditions and that the Fe-bearing minerals present the main control. Commonly, the combinations of these minerals that we observe within serpentinites, in order of formation, are brucite, brucite + awaruite, and awaruite + magnetite, which implies that awaruite + magnetite-bearing serpentinites may evolve from brucite-bearing serpentinites via a trajectory similar to that shown (A–B–C–E). On this trajectory, brucite is the first Fe-bearing phase to form after olivine hydration. If brucite formation occurs at the same time as the formation of Fe^{3+}-bearing serpentinite, then the aH$_2$ of the fluid would increase (A–B) until the system encountered the brucite–awaruite reaction at B, at which point, depending on fluid composition and water: rock ratios, the system might proceed up or down the brucite–awaruite buffer towards C or D, respectively. If the system evolves towards awaruite-free assemblages than low fO$_2$ and low fS$_2$ may not occur. For example, serpentine–brucite–magnetite is a common assemblage within serpentinite veins and this assemblage does not constrain the fluid to be extremely reducing (Frost, 1985).

Here, we consider how the system might proceed to the magnetite–awaruite buffer (B–C–E), because this sequence of assemblages is observed in rocks (Table 1). Magnetite–awaruite is stable at lower aH$_2$ and aH$_2$O than the brucite–awaruite reaction, so a process to reduce both aH$_2$ and aH$_2$O of the system must occur if the rock is to lose brucite. At first sight, this appears difficult to explain if the system remains fluid-bearing and if H_2 and H_2O are the main fluid species, because, if xH$_2$ + xH$_2$O = 1 then they cannot decrease at the same time unless the activity–composition relationships are more non-ideal than is generally recognised. However, other fluid species, such as Na^+ or Cl^-, may increase in concentration as H_2O is consumed by ongoing serpentinisation, reducing the mole fraction and activity of H_2O (e.g., Scambelluri et al., 1997). Another possibility is that the free fluid phase is consumed during some parts of the rock's serpentinisation history, which would decrease the activity of H_2O and H_2 simultaneously. Both these possibilities are consistent with episodic fluid infiltration, which is documented by the complex laminated vein systems shown by many serpentinites, and consistent with the suggestion of Sciortino et al. (2015) that low aH$_2$O was a factor in the formation of awaruite during serpentinisation of the Dumont Sill.

Of course, Fig. 5 is schematic, and neglects the effects of the non-Fe components within magnetite, awaruite, and brucite. The effect of these components is to broaden the lines into fields or volumes within composition space, and the distribution and relative stabilities of the phases are sensitive to a wide range of parameters (Fig. 6). However, the general trends should remain robust. Further, the evolution from brucite, through brucite + awaruite to brucite + magnetite is only one of the diverse sequences of mineral assemblages observed within serpentinites. The trajectory and consequent sequence of assemblages depends to a large extent on factors such as temperature, which affect the partitioning of Fe^{3+} between silicate and oxide phases. For example, low temperatures favour the formation of Fe^{3+}-bearing serpentine over magnetite because the volatile content and entropy production of the reaction are lower than for magnetite-forming reactions. If reduction in aH$_2$O is a factor (Figs. 5, 6), then the trajectory also depends on the instantaneous fluid:rock ratio because internal rock buffering is stronger at low water: rock ratios so the system will be relatively mobile along the lines and points that define low-variance reactions, such as the simplified versions shown on Fig. 5. If the instantaneous fluid:rock ratio is higher, then the system will show a greater degree of external buffering with respect to fluid composition and mobility of the system within fluid composition space will be more limited.

Awaruite is commonly reported, along with a range of PGE alloys interpreted to record desulfidation of PGE-hosting sulfides, from serpentinised chromites (e.g., Table 1, (Airiyants et al., 2022; Gonzalez-Jimenez et al., 2010; Graham et al., 1996; Jiang and Zhu, 2020). Here awaruite typically coexists with ferrit-chromite after chromite, so it is plausible that the requirement for formation of an Fe-rich, Si-poor phase drove disproportionation of Fe^{2+} to form Fe^{3+} in ferrit-chromite and Fe^0 in awaruite, and H_2 production, as described above. The difference between the formation of ferrit-chromite and the formation of magnetite is that the formation of Fe^{3+}- and Cr^{3+}-bearing spinel is facilitated by the potential to form a solid solution between Cr-bearing spinel and Fe^{3+}-bearing spinel, reducing the required activity of magnetite for the reaction to proceed (e.g., Girardi et al., 2006).

In more Ca-rich systems, such as those associated with rodingitized dykes, Fe derived from olivine breakdown may be incorporated into andradite as Fe^{3+}. The requirement for an electron acceptor drives H_2 formation from water and provides a mechanism to disproportionate Fe^{2+} to form Fe^0 within awaruite and Fe^{3+} within andradite (Beard and Hopkinson, 2000). The coexistence of andradite or hydro-andradite with awaruite has been reported from a range of serpentinites where Ca-rich fluids are present under reducing and Si-poor conditions, including the Josephine Ophiolite, where large nuggets of intergrown awaruite and andradite are recorded (e.g., Frost, 1985; Plumper et al., 2014; Templeton et al., 2021). Not all Ca-bearing systems follow this trajectory, Lost City vent fluids are consistent with equilibrium with serpentine, diopside, and tremolite or anhydrite, and inconsistent with brucite stability, reflecting higher SiO_2 activities that those required for alloy formation (Seyfried et al., 2015). It is possible to construct a simplified illustration of the complex relationships amongst the parameters that determine the fate of Fe released by olivine serpentinisation (Fig. 7), and the textural features that record these relationships (Fig. 8).

In other cases, other electron acceptors may be active. For example, carbon-rich ultramafic rocks from ophiolites of the Ospa-Kitoi area, East Sayan, Siberia, host abundant awaruite as well as PGE-alloys and other PGMs (Zhmodik et al., 2004). Fluid inclusions are dominated by methane, and carbon is thought to have been sourced from the mantle or the adjacent black-shale deposits. Secondary CH_4-bearing fluid inclusions within olivine have also been reported from a wide range of geological settings, where CH_4, probably sourced from C dissolved in seawater, coexists with awaruite, serpentine, brucite, magnetite, and H_2 (Klein et al., 2019). Regardless of the source, carbon acts as an electron donor during the formation of graphite from methane, which favouring formation of awaruite.

Another unusual case that provides insights into the process is the coexisting Fe-bearing monticellite, magnetite, and awaruite described by Nozaka (2020). Monticellite replaces typical mantle olivine (X(Mg) ~ 0.9) in response to infiltration of Ca-bearing fluids, and the association between monticellite and awaruite supports formation of awaruite from Ni- and Fe- from the original olivine. Coexisting magnetite, although this is not noted as inclusions within the monticellite, may record disproportionation of Fe^{2+} from olivine to form Fe^0 in awaruite and Fe^{3+} in magnetite.

5.4. Links to low sulfur fugacity

The mechanism discussed above explains low fS_2 without any need for the sulfides to form the main driver of the process or control fO_2. Oxidised and reduced S in metamorphic fluids are related by the expression of the form $2\ SO_2 + 2\ H_2O = 2\ H_2S + 3\ O_2$. The fugacities of SO_2 and H_2S are equal at conditions referred to as the sulfide–sulfate fence, or SSO. At temperatures of serpentinisation, SSO lies at fO_2 well above the fayalite–magnetite–quartz (FMQ) buffer and approaches the hematite–magnetite (HM) buffer at low temperature (Fig. 9). Thus, one can confidently assert that the major sulfur species is H_2S during serpentinisation. Under these conditions, in the presence of H_2O, the fugacities of sulfur and oxygen are related by the expression: $S_2 + 2\ H_2O = H_2S + O_2$. Thus, in the stability field of H_2S, decreasing fO_2 is associated with decreasing fS_2, which destabilizes sulfides. Conversely, fS_2 increases as fO_2 increases, consistent with the observation that new-formed sulfides, such as polydymite and pyrite, are common within serpentinites (Table 1), but the extent of new sulfide growth depends on the S content of the fluid. Stable assemblages of S-bearing minerals calculated as a function of aS_2 and fO_2 (Fig. 4) show a diverse range of textures and assemblages that document the overgrowth of alloys by sulfide and oxides (Fig. 10).

Thus, desulfidation is a response to reducing conditions imposed by olivine hydration reactions and the link between fO_2 and fS_2 rather than the primary cause of low fO_2, consistent with the relatively low S contents of most serpentinites, which are generally <0.2 wt%, in contrast with FeO_{tot} contents that are one to two orders of magnitude higher.

5.5. Comparison with other mechanisms suggested for awaruite formation

It has been suggested that fluctuating conditions are integral to the coexistence of awaruite with Fe^{3+}-bearing minerals. For example, podiform chromitites from Veria, Greece host awaruite, heazlewoodite, undescribed carbon-bearing material, and oxides that are associated with Fe-chromite and andradite-uvavorite garnets (Tsoupas and Economou-Eliopoulos, 2021). These authors attribute the presence of awaruite and Fe^{3+}-bearing garnet to a shift from reducing to oxidizing conditions, but this is not necessary to explain the mineral associations. Similarly, Franklin et al. (1992) suggested that coexisting ferritchromite and awaruite within chromites from the Coolac Serpentinite Belt, New South Wales, require variation in redox conditions to explain their formation. However, if Fe^{2+} from olivine disproportionates to form Fe^0 and Fe^{3+} then these fluctuating conditions are not required.

A model to explain the coexistence of brucite and awaruite, which coexist in all awaruite-bearing samples from 15′20 Fracture Zone, was proposed by Klein and Bach (2009). These authors note that brucite–olivine coexistence buffers $aSiO_2$ to very low values, but also that brucite stability facilitates the formation of H_2, which causes awaruite formation under H_2S-buffered conditions. While the observations are of the highest quality, brucite stability alone does not facilitate the formation of H_2 or provide a clear mechanism to do so. Instead, we propose that brucite stability is accompanied by the formation of Fe-bearing serpentinite, that some of the Fe incorporated into serpentine is ferric, and that this is the process that drives the formation of H_2 and Fe disproportionation to form awaruite.

6. Outlook

The study of alloys has historically been hindered by their small size, opacity, and a lack of detail around textural relationships, but modern high spatial resolution and automated mapping techniques facilitate their recognition and analysis. These techniques reveal that awaruite, native Cu-alloys, and PGE alloys are relatively common within hydrated ultramafic rocks.

The formation of alloys during serpentinisation provides a fascinating example of the complexity that systems with a relatively small number of major components can show. A diverse range of assemblages, sequences of assemblages, and mineral compositions occur within different tectonic environments in response to differences in externally controlled variables (P, T, water:rock ratios), that lead to different trajectories within $aSiO_2$–aH_2–aH_2O–aS_2 (and other variables) space. However, this review highlights similarities amongst the diverse alloy-forming environments. Some of these, such as the low fO_2 and fS_2, and the common observation of low water:rock ratios, are relatively well known. Others, such as the ubiquitous presence of a Fe^{3+}-bearing phase, which requires some combination of the disproportionation of Fe^{2+} and the formation of H_2, which can act as an electron donor elsewhere within the system, are less well recognised. Further, potentially important factors such as low aH_2O and the importance of electron acceptors other than water-borne H+ require further investigation.

The relative stability of PGE, Cu, and Fe-Ni alloys also requires further investigation. Clearly, native Cu is stable across a broader range of conditions than the Fe-Ni alloys, but it would be useful to be able to quantify the stability of a broad range of PGE and BM alloys as a function of intensive and extensive variables. This requires new thermodynamic data and activity composition models for all but the most common alloys, and better characterisation of alloy compositions. A better understanding of alloy stability would enable better predictions of the conditions and length scales of PGE and BM mobility, with consequences for techniques such as Re-Os geochronology and new insights into the processes that formed large awaruite nuggets, such as those at the Baptiste Deposit and the Josephine Ophiolite. Further, a better understanding of environments where alloys can act as catalysts, and the compositional ranges of alloys, might have applications within the material sciences and implications for our understanding of early Earth and life on Earth and other planets.

Declaration of Competing Interest

Katy Evans reports financial support was provided by Australian Research Council. Steve Reddy reports financial support was provided by Australian Research Council. Ron Frost reports financial support was provided by The Institute for Geoscience Research.

Acknowledgements

The authors would like to thank TiGeR (The Institute for Geoscience Research) for funding for B.R. Frost to visit Australia in 2018. K. Evans and S. Reddy are supported by ARC Discovery Grants DP210101866 and DP210102625. Henry Dick is thanked for the josephinite samples. Thanks to Blackstone Minerals for samples shown in the photomicrographs and BSE images in Fig. 10. Frieder Klein is thanked for his patient knowledgeable editing, and Ron Britten and an anonymous reviewer are thanked for insightful comments that helped us to improve the manuscript.

References

Airiyants, E.V., Kiseleva, O.N., Zhmodik, S.M., Belyanin, D.K., Ochirov, Y.C., 2022. Platinum-group minerals in the placer of the Kitoy River, East Sayan, Russia. Minerals 12.

Alard, O., Lorand, J.P., Reisberg, L., Bodinier, J.L., Dautria, J.M., O'Reilly, S.Y., 2011. Volatile-rich metasomatism in Montferrier xenoliths (Southern France): Implications for the abundances of chalcophile and highly siderophile eements in the subcontinental mantle. J. Petrol. 52, 2009–2045.

Alt, J.C., Shanks, W.C., 1998. Sulfur in serpentinized oceanic peridotites: Serpentinization processes and microbial sulfate reduction. J. Geophys. Res. Solid Earth 103, 9917–9929.

Auge, T., Cabri, L.J., Legendre, O., McMahon, G., Cocherie, A., 1999. PGE distribution in base-metal alloys and sulfides of the New Caledonia ophiolite. Can. Mineral. 37, 1147–1161.

Beard, J.S., Hopkinson, L., 2000. A fossil, serpentinization-related hydrothermal vent, Ocean Drilling Program Leg 173, Site 1068 (Iberia Abyssal Plain): some aspects of mineral and fluid chemistry. J. Geophys. Res. Solid Earth 105, 16527–16539.

Beard, J.S., Frost, B.R., Fryer, P., McCaig, A., Searle, R., Ildefonse, B., Zinin, P., Sharma, S.K., 2009. Onset and progression of serpentinization and magnetite formation in olivine-rich troctolite from IODP hole U1309D. J. Petrol. 50, 387–403.
Becker, H., Dale, C.W., 2016. Re-Pt-Os isotopic and highly siderophile element behavior in oceanic and continental mantle tectonites. In: Harvey, J., Day, J.M.D. (Eds.), Highly Siderophile and Strongly Chalcophile Elements in High-Temperature Geochemistry and Cosmochemistry, pp. 369–440.
Beinlich, A., von Heydebrand, A., Klemd, R., Martin, L., Hicks, J., 2020. Desulphurisation, chromite alteration, and bulk rock PGE redistribution in massive chromitite due to hydrothermal overprint of the Panton Intrusion, east Kimberley, Western Australia. Ore Geol. Rev. 118.
Bina, M.M., Henry, B., 1990. Magnetic-properties, opaque mineralogy and magnetic anisotropies of serpentinized peridotites from ODP Hole 670A near the Mid-Atlantic Ridge. Phys. Earth Planet. Inter. 65, 88–103.
Bonazzi, P., Bindi, L., 2021. Structural and chemical characterization of dienerite, Ni_3As, and its revalidation as a mineral species. Can. Mineral. 59, 1887–1898.
Botto, R.I., Morrison, G.H., 1976. Josephinite - unique nickel-iron. Am. J. Sci. 276, 241–274.
Bowles, J.F.W., Gize, A.P., Vaughan, D.J., Norris, S.J., 1994. Development of platinum-group minerals in laterites - initial comparison of organic and inorganic controls transactions of the Institution of Mining and Metallurgy Section B-Applied. Earth Sci. 103, B53–B56.
Bowles, J.F.W., Prichard, H.M., Suarez, S., Fisher, P.C., 2013. The first report of platinum-group minerals in magnetite-bearing gabbro, Freetown layered complex, Sierra Leone: Occurences and genesis. Can. Mineral. 51, 455–473.
Bowles, J.F.W., Suarez, S., Prichard, H.M., Fisher, P.C., 2017. Weathering of PGE sulfides and Pt-Fe alloys in the Freetown Layered Complex, Sierra Leone. Mineral. Deposita 52, 1127–1144.
Brathwaite, R.L., Christie, A.B., Jongens, R., 2017. Chromite, platinum group elements and nickel mineralisation in relation to the tectonic evolution of the Dun Mountain Ophiolite Belt, east Nelson, New Zealand. N. Z. J. Geol. Geophys. 60, 255–269.
Britten, R., 2017. Regional metallogeny and genesis of a new deposit type-disseminated awaruite (Ni_3Fe) mineralization hosted in the Cache Creek Terrane. Econ. Geol. 112, 517–550.
Cabral, A.R., Galbiatti, H.F., Kwitko-Ribeiro, R., Lehmann, B., 2008. Platinum enrichment at low temperatures and related microstructures, with examples of hongshiite (PtCu) and empirical 'Pt_2HgSe_3' from Itabira, Minas Gerais, Brazil. Terra Nova 20, 32–37.
Challis, G.A., 1975. Native nickel from the Jerry River, South Westland, New Zealand: an example of natural refining. Mineral. Mag. 40, 247–251.
Clark, A.L., Greenwood, W.R., 1972. Geochemistry and distribution of platinum group metals in mafic to ultramafic conplexes of southern and southeastern Alaska. United States Geol. Surv. Res. 1972, 157–160.
Crossley, R.J., Evans, K.A., Evans, N.J., Bragagni, A., McDonald, B.J., Reddy, S.M., Speelmanns, I.M., 2020. Tracing highly siderophile elements through subduction: Insights from high-pressure serpentinites and 'hybrid' rocks from Alpine Corsica. J. Petrol. 61.
Daly, L., Bland, P.A., Dyl, K.A., Forman, L.V., Evans, K.A., Trimby, P.W., Moody, S., Yang, L.M., Liu, H.W., Ringer, S.P., Ryan, C.G., Saunders, M., 2017. In situ analysis of refractory metal nuggets in carbonaceous chondrites. Geochim. Cosmochim. Acta 216, 61–81.
Day, J.M.D., Brandon, A.D., Walker, R.J., 2016. Highly siderophile elements in Earth, Mars, the Moon, and asteroids. In: Harvey, J., Day, J.M.D. (Eds.), Highly Siderophile and Strongly Chalcophile Elements in High-Temperature Geochemistry and Cosmochemistry, pp. 161–238.
Dick, H.J.B., 1974. Terrestrial nickel-iron from the Josephine Peridotite, its geologic occurrence, associations, and origin. Earth Planet. Sci. Lett. 24, 291–298.
Eckstrand, O.R., 1975. The Dumont serpentinite; a model for control of nickeliferous opaque mineral assemblages by alteration reactions in ultramafic rocks. Econ. Geol. 70, 183–201.
Ellison, E.T., Templeton, A.S., Zeigler, S.D., Mayhew, L.E., Kelemen, P.B., Matter, J.M., Oman Drilling Project Sci, P, 2021. Low-temperature hydrogen formation during aqueous alteration of serpentinized peridotite in the Samail Ophiolite. Journal of Geophysical Research-Solid. Earth 126.
Escayola, M., Garuti, G., Zaccarini, F., Proenza, J.A., Bedard, J.H., Van Staal, C., 2011. Chromitite and platinum-group-element mineralization at Middle Arm Brook, Central Advocate Ophiolite complex, Baie Verte Peninsula, Newfoundland, Canada. Can. Mineral. 49, 1523–1547.
Evans, K.A., Frost, B.R., 2021. Deserpentinization in subduction zones as a source of oxidation in arcs: a reality check. J. Petrol. 62, 1–32.
Evans, B.W., Kuehner, S.M., Chopelas, A., 2009. Magnetite-free, yellow lizardite serpentinization of olivine websterite, Canyon Mountain complex, NE Oregon. Am. Mineral. 94, 1731–1734.
Evans, K.A., Powell, R., Frost, B.R., 2013. Using equilibrium thermodynamics in the study of metasomatic alteration, illustrated by an application to serpentinites. Lithos 168-169, 67–84.
Evans K.A., Reddy S.M., Merle R.E., Fougerouse D., Rickard W.D.A., Saxey D., Park J.W., Doucet L., Jourdan F., The origin of platinum group minerals in oceanic crust. Geology. (In press).
Evans, K.A., Reddy, S.M., Tomkins, A.G., Crossley, R.J., Frost, B.R., 2017. Effects of geodynamic setting on the redox state of fluids released by subducted mantle lithosphere. Lithos 278-281, 26–42.
Fonseca, R.O.C., Laurenz, V., Mallmann, G., Luguet, A., Hoehne, N., Jochum, K.P., 2012. New constraints on the genesis and long-term stability of Os-rich alloys in the Earth's mantle. Geochim. Cosmochim. Acta 87, 227–242.
Foustoukos, D.I., 2019. Hydrothermal oxidation of Os. Geochim. Cosmochim. Acta 255, 237–246.
Foustoukos, D.I., Bizimis, M., Frisby, C., Shirey, S.B., 2015. Redox controls on Ni-Fe-PGE mineralization and Re/Os fractionation during serpentinization of abyssal peridotite. Geochim. Cosmochim. Acta 150, 11–25.
Franklin, B.J., Marshall, B., Graham, I.T., McAndrew, J., 1992. Remobilisation of PGE in podiform chromitite in the Coolac Serpentite Belt, Southeastern Australia. Aust. J. Earth Sci. 39, 365–371.
Frost, B.R., 1985. On the stability of sulfides, oxides, and native metals in serpentinite. J. Petrol. 26, 31–63.
Frost, R.B., Beard, J.S., 2007. On silica activity and serpentinization. J. Petrol. 48, 1351–1368.
Frost, B.R., Beard, J.S., McCaig, A., Condliffe, E., 2008. The formation of micro-rodingites from IODP hole U1309D: Key to understanding the process of serpentinization. J. Petrol. 49, 1579–1588.
Frost, B.R., Evans, K.A., Swapp, S.M., Beard, J.S., Mothersole, F.E., 2013. The process of serpentinization in dunite from New Caledonia. Lithos 178, 24–39.
Fuchs, W.A., Rose, A.W., 1974. Geochemical behavior of platinum and palladium in weathering cycle in Stillwater complex, Montana. Econ. Geol. 69, 332–346.
Garuti, G., Zaccarini, F., 1997. In situ alteration of platinum-group minerals at low temperature: evidence from serpentinized and weathered chromitite of the Vourinos complex, Greece. Can. Mineral. 35, 611–626.
Girardi, V.A.V., Ferrario, A., Correia, C.T., Diella, V., 2006. A comparison of selected Precambrian Brazilian chromitites: Chromite, PGE-PGM, and Re/Os as parental source indicators. J. S. Am. Earth Sci. 20, 303–313.
Gonzalez-Jimenez, J.M., Gervilla, F., Kerestedjian, T., Proenza, J.A., 2010. Alteration of platinum-group and base-metal mineral assemblages in ophiolite chromitites from the Dobromirtsi Massif, Rhodope Mountains (Bulgaria). Resour. Geol. 60, 315–334.
Gonzalez-Jimenez, J.M., Auge, T., Gervilla, F., Bailly, L., Proenza, J.A., Griffin, W.L., 2011. Mineralogy and geochemistry of platinum-rich chromitites from the mantle-crust transition zone at Ouen Island, New Caledonia Ophiolite. Can. Mineral. 49, 1549–1569.
Gonzalez-Jimenez, J.M., Pina, R., Saunders, J.E., Plissart, G., Marchesi, C., Padron-Navarta, J.A., Ramon-Fernandez, M., Garrido, L.N.F., Gervilla, F., 2021. Trace element fingerprints of Ni-Fe-S-As minerals in subduction channel serpentinites. Lithos 400.
Graham, I.T., Franklin, B.J., Marshall, B., 1996. Chemistry and mineralogy of podiform chromitite deposits, southern NSW, Australia: a guide to their origin and evolution. Mineral. Petrol. 57, 129–150.
Hanley, J.J., Pettke, T., Mungall, J.E., Spooner, E.T.C., 2005. The solubility of platinum and gold in NaCl brines at 1.5 kbar, 600 to 800°C: a laser ablation ICP-MS pilot study of synthetic fluid inclusions. Geochim. Cosmochim. Acta 69, 2593–2611.
Harrison, A.L., Power, I.M., Dipple, G.M., 2013. Accelerated Carbonation of Brucite in Mine Tailings for Carbon Sequestration. Environ. Sci. Technol. 47, 126–134.
Harvey, J., Warren, J.M., Shirey, S.B., 2016. Mantle sulfides and their role in Re-Os and Pb isotope geochronology. In: Harvey, J., Day, J.M.D. (Eds.), Highly Siderophile and Strongly Chalcophile Elements in High-Temperature Geochemistry and Cosmochemistry, pp. 579–649.
Haxel, G.B., Wittke, J.H., Epstein, G.S., Jacobson, C.E., 2018. Serpentinization-related nickel, iron, and cobalt sulfide, arsenide, and intermetallic minerals in an unusual inland tectonic setting, southern Arizona, USA. In: Ingersoll, R.V., Lawton, T.F., Graham, S.A. (Eds.), Tectonics, Sedimentary Basins, and Provenance: A Celebration of the Career of William R. Dickinson, pp. 65–87.
Herzberg, C., Vidito, C., Starkey, N.A., 2016. Nickel-cobalt contents of olivine record origins of mantle peridotite and related rocks. Am. Mineral. 101, 1952–1966.
Horita, J., Berndt, M.E., 1999. Abiogenic methane formation and isotopic fractionation under hydrothermal conditions. Science 285, 1055–1057.
Howald, R.A., 2003. The thermodynamics of tetrataenite and awaruite: A review of the Fe-Ni phase diagram. Metallurgical and Materials Transactions a-Physical Metallurgy and Materials Science 34A, 1759–1769.
Jamieson, G.S., 1905. On the natural iron-nickel alloy, awaruite. Am. J. Sci. 4, 413–415.
Jiang, J.Y., Zhu, Y.F., 2020. Characterization of the Hegenshan podiform chromitites (Inner Mongolia, China): Sub-solidus cooling and hydrothermal alteration. Ore Geol. Rev. 120.
Jimenez-Franco, A., Gonzalez-Jimenez, J.M., Roque, J., Proenza, J.A., Gervilla, F., Nieto, F., 2020. Nanoscale constraints on the in situ transformation of Ru-Os-Ir sulfides to alloys at low temperature. Ore Geol. Rev. 124.
Johan, Z., 2002. Alaskan-type complexes and their Platinum-group element mineralization. In: Cabri, L.J. (Ed.), The Geology, Geochemistry, Mineralogy and Beneficiation of the Platinum-group Elements. Canadian Institute of Mining, Metallurgy, and Petroleum, pp. 669–720.
Kakefuda, M., Tsujimori, T., Yamashita, K., Iizuka, Y., Flores, K.E., 2020. Revisiting Pb isotope signatures of Ni-Fe alloy hosted by antigorite serpentinite from the Josephine Ophiolite, USA. J. Mineral. Petrol. Sci. 115, 21–28.
Klein, F., Bach, W., 2009. Fe-Ni-Co-O-S phase relations in peridotite-seawater interactions, 50, pp. 37–59.
Klein, F., Bach, W., Jöns, N., McCollom, T., Moskowitz, B., Berquó, T., 2009. Iron partitioning and hydrogen generation during serpentinization of abyssal peridotites from 15°N on the Mid-Atlantic Ridge., 73, p. 6893.
Klein, F., Bach, W., Humphris, S.E., Kahl, W.A., Jöns, N., Moskowitz, B., Berquó, T.S., 2014. Magnetite in seafloor serpentinite-Some like it hot. Geology 42, 135–138.
Klein, F., Grozeva, N.G., Seewald, J.S., 2019. Abiotic methane synthesis and serpentinization in olivine-hosted fluid inclusions. Proceedings of the National Academy of Sciences of the United States of America 116, 17666–17672.
Kutyrev, A.V., Sidorov, E.G., Kamenetsky, V.S., Chubarov, V.M., Chayka, I.F., Abersteiner, A., 2021. Platinum mineralization and geochemistry of the Matysken

zoned Ural-Alaskan type complex and related placer (Far East Russia). Ore Geol. Rev. 130.
Lawley, C.J.M., Petts, D.C., Jackson, S.E., Zagorevski, A., Pearson, D.G., Kjarsgaard, B.A., Savard, D., Tschirhart, V., 2020. Precious metal mobility during serpentinization and breakdown of base metal sulphide. Lithos 354.
Lorand, J.P., 1989. Mineralogy and chemistry of Cu-Fe-Ni sulfides in orogenic-type spinel peridotite bodies from Ariege (Northeastern Pyrenees, France). Contrib. Mineral. Petrol. 103, 335–345.
Lorand, J.P., Luguet, A., 2016. Chalcophile and siderophile elements in mantle rocks: trace elements controlled By trace minerals. In: Harvey, J., Day, J.M.D. (Eds.), Highly Siderophile and Strongly Chalcophile Elements in High-Temperature Geochemistry and Cosmochemistry, pp. 441–488.
McCollom, T.M., Seewald, J.S., 2001. A reassessment of the potential for reduction of dissolved CO_2 to hydrocarbons during serpentinization of olivine. Geochim. Cosmochim. Acta 65, 3769–3778.
McCollom, T.M., Seewald, J.S., 2006. Carbon isotope composition of organic compounds produced by abiotic synthesis under hydrothermal conditions. Earth Planet. Sci. Lett. 243, 74–84.
Milidragovic, D., Nixon, G., Scoates, J.S., Nott, J.A., Spence, D.W., 2021. Redox-controlled chalcophile element geochemistry of the Polaris Alaskan-Type mafic-ultramafic complex, British Columbia, Canada. Can. Mineral. 59, 1627–1660.
Neto-Lima, J., Fernandez-Sampedro, M., Prieto-Ballesteros, O., Iop, 2015. High pressure serpentinization catalysed by awaruite in planetary bodies. In: Joint 25th AIRAPT / 53rd EHPRG International Conference on High Pressure Science and Technology, Madrid, SPAIN.
Nozaka, T., 2003. Compositional heterogeneity of olivine in thermally metamorphosed serpentinite from Southwest Japan. Am. Mineral. 88, 1377–1384.
Nozaka, T., 2020. Fe-monticellite in serpentinites from the Happo ultramafic complex. Lithos 374.
O'Driscoll, B., Gonzalez-Jimenez, J.M., 2016. Petrogenesis of the platinum-group minerals. In: Harvey, J., Day, J.M.D. (Eds.), Highly Siderophile and Strongly Chalcophile Elements in High-Temperature Geochemistry and Cosmochemistry, pp. 489–578.
Parman, S.W., Diercks, D.R., Gorman, B.P., Cooper, R.F., 2015. Atom probe tomography of isoferroplatinum. Am. Mineral. 100, 852–860.
Paulick, H., Bach, W., 2006. Phyllosilicate alteration mineral assemblages in the active subsea-floor Pacmanus hydrothermal system, Papua New Guinea, ODP Leg 193. Econ. Geol. 101, 633–650.
Paulick, H., Bach, W., Godard, M., De Hoog, J.C.M., Suhr, G., Harvey, J., 2006. Geochemistry of abyssal peridotites (Mid-Atlantic Ridge, 15°20′N, ODP Leg 209): Implications for fluid/rock interaction in slow spreading environments. Chem. Geol. 234, 179–210.
Peretti, A., Dubessy, J., Mullis, J., Frost, B.R., Trommsdorff, V., 1992. Highly reducing conditions during Alpine metamorphism of the Malenco peridotite (Sondrio, northern Italy) indicated by mineral paragenesis and H2 in fluid inclusions. Contrib. Mineral. Petrol. 112, 329–340.
Plumper, O., Beinlich, A., Bach, W., Janots, E., Austrheim, H., 2014. Garnets within geode-like serpentinite veins: Implications for element transport, hydrogen production and life-supporting environment formation. Geochim. Cosmochim. Acta 141, 454–471.
Prichard, H.M., Neary, C.R., Fisher, P.C., O'Hara, M.J., 2008. PGE-rich podiform chromitites in the Al 'Ays Ophiolite Complex, Saudi Arabia: an example of critical mantle melting to extract and concentrate PGE. Econ. Geol. 103, 1507–1529.
Rajendran, S., Nasir, S., 2014. Hydrothermal altered serpentinized zone and a study of Ni-magnesioferrite-magnetite-awaruite occurrences in Wadi Hibi, Northern Oman Mountain: Discrimination through ASTER mapping. Ore Geol. Rev. 62, 211–226.
Ramdohr, P., 1950. Über Josephinit, Awaruit, Souesit, ihre Eigenschaften, Entstehung und Paragenesis. Mineral. Mag. 29, 374–394.
Salters, V.J.M., Stracke, A., 2004. Composition of the depleted mantle. Geochem. Geophys. Geosyst. 5.
Scambelluri, M., Piccardo, G.B., Philippot, P., Robbiano, A., Negretti, L., 1997. High salinity fluid inclusions formed from recycled seawater in deeply subducted alpine serpentinite. Earth Planet. Sci. Lett. 148, 485–499.
Schwarzenbach, E.M., Gazel, E., Caddick, M.J., 2014. Hydrothermal processes in partially serpentinized peridotites from Costa Rica: evidence from native copper and complex sulfide assemblages. Contrib. Mineral. Petrol. 168.
Schwarzenbach, E.M., Vrijmoed, J.C., Engelmann, J.M., Liesegang, M., Wiechert, U., Rohne, R., Plumper, O., 2021. Sulfide dissolution and awaruite formation in continental serpentinization environments and its implications to supporting life. J. Geophys. Res. Solid Earth 126.
Sciortino, M., Mungall, J.E., Muinonen, J., 2015. Generation of high-Ni sulfide and alloy phases during serpentinization of dunite in the dumont sill, Quebec. Econ. Geol. 110, 733–761.
Scott, P.W., Jackson, T.A., Dunham, A.C., 1999. Economic potential of the ultramafic rocks of Jamaica and Tobago: two contrasting geological settings in the Caribbean. Mineral. Deposita 34, 718–723.
Seiler, S., Sanchez, G., Teliz, E., Diaz, V., 2022. Awaruite (Ni_3Fe), a new large nickel resource: Electrochemical characterization and surface composition under flotation-related conditions. Miner. Eng. 184.
Seyfried, W.E., Foustoukos, D.I., Fu, Q., 2007. Redox evolution and mass transfer during serpentinization: an experimental and theoretical study at 200 degrees C, 500 bar with implications for ultramafic-hosted hydrothermal systems at Mid-Ocean Ridges. Geochim. Cosmochim. Acta 71, 3872–3886.
Seyfried, W.E., Pester, N.J., Tutolo, B.M., Ding, K., 2015. The Lost City hydrothermal system: Constraints imposed by vent fluid chemistry and reaction path models on subseafloor heat and mass transfer processes. Geochim. Cosmochim. Acta 163, 59–79.
Sleep, N.H., Meibom, A., Fridriksson, T., Coleman, R.G., Bird, D.K., 2004. H-2-rich fluids from serpentinization: Geochemical and biotic implications. Proc. Natl. Acad. Sci. U. S. A. 101, 12818–12823.
Syverson, D.D., Tutolo, B.M., Borrok, D.M., Seyfried, W.E., 2017. Serpentinization of olivine at 300 degrees C and 500 bars: an experimental study examining the role of silica on the reaction path and oxidation state of iron. Chem. Geol. 475, 122–134.
Templeton, A.S., Ellison, E.T., Glombitza, C., Morono, Y., Rempfert, K.R., Hoehler, T.M., Zeigler, S.D., Kraus, E.A., Spear, J.R., Nothaft, D.B., Fones, E.M., Boyd, E.S., Munro-Ehrlich, M., Mayhew, L.E., Cardace, D., Matter, J.M., Kelemen, P.B., Oman Drilling Project Sci, P, 2021. Accessing the subsurface biosphere within rocks undergoing active low-temperature serpentinization in the Samail Ophiolite (Oman Drilling Project). J. Geophys. Res. Biogeosci. 126.
Tsoupas, G., Economou-Eliopoulos, M., 2021. Transformation of PGM in supra subduction zones: Geochemical and mineralogical constraints from the Veria (Greece) podiform chromitites. Geosci. Front. 12, 827–842.
Tutolo, B.M., Seyfried, W.E., Tosca, N.J., 2020. A seawater throttle on H-2 production in Precambrian serpentinizing systems. Proc. Natl. Acad. Sci. U. S. A. 117, 14756–14763.
Uysal, I., Akmaz, R.M., Kapsiotis, A., Demir, Y., Saka, S., Avci, E., Muller, D., 2015. Genesis and geodynamic significance of chromitites from the Orhaneli and Harmancik ophiolites (Bursa, NW Turkey) as evidenced by mineralogical and compositional data. Ore Geol. Rev. 65, 26–41.
Warr, L.N., 2021. IMA-CNMNC approved mineral symbols. Mineral. Mag. 85, 291–320.
Wood, S.A., 1991. Experimental-determination of the hydrolysis constants of Pt2+ and Pd2+ at 25-degrees-C from the solubility of Pt and Pd in aqueous hydroxide solutions. Geochim. Cosmochim. Acta 55, 1759–1767.
Yurichev, A.N., Chenyshov, A.I., Korbovyak, E.V., 2021. New data on the platinum-bearing potential of chromitites of the Kharcheruz Ultramafic Massif, Polar Urals. Geol. Ore Deposits 63, 705–716.
Zhmodik, S.M., Mironov, A.G., Agafonov, L.V., Zhmodik, A.S., Pavlov, A.L., Moroz, T.N., Airiyants, E.V., Kulikov, Y.I., Borovikov, A.A., Ponomarchuk, V.A., Damdinov, B.B., 2004. Carbonization of East Sayan ultrabasic rocks and Au-Pd-Pt mineralization. Geol. Geofiz. 45, 228–243.